# Unlocking the correlation in fluvial outcrops by using a DOM-derived Virtual Datum: Method description and field tests in the Huesca Fluvial Fan, Ebro Basin (Spain)

**Rubén Calvo[1] and Emilio Ramos[1]**

[1]*GEOMODELS Institute, Group of Geodynamics and Basin Analysis (GGAC), Dept. of Stratigraphy, Paleontology and Marine Geosciences, University of Barcelona, Barcelona 08028, Spain. ruben.calvo@ub.edu; emilio.ramos@ub.edu*

**ABSTRACT**

Adequate characterization of depositional architecture is of great importance when studying fluvial outcrops as reservoir analogs. The complex three-dimensional (3D) distribution and lateral/vertical relationships of sandstone bodies require a high degree of stratigraphic control in order to make a proper assessment of the distribution and connectivity of the reservoir facies. This demands the use of reliable correlation datums. Unfortunately, clear marker beds (e.g., ash/coal layers and paleosols) are not always available in fluvial outcrops, and when present they are often covered by vegetation or debris that prevents their tracking over long distances.

A new method to achieve highly accurate and semiautomatic correlations within fluvial DOMs (Digital Outcrop Model) is presented in response to the need for further correlation procedures, especially in the absence of suitable datums. The method is based on the hypothesis that the average depositional paleosurface of a sedimentary system can be represented by a plane at outcrop scale. If this assumption is valid, this plane can be used as a Virtual Datum to identify along the DOM the sediments that were deposited simultaneously.

The method was tested and applied successfully within two kilometer-scale outcrops of the Huesca Fluvial Fan (Early Miocene, N Spain), where the Virtual Datum provided

accurate correlations regardless of stratigraphic or topographical complexities. Moreover, the entire sedimentary successions were automatically subdivided into the desired stratigraphic intervals by only moving the Virtual Datum vertically. These intervals can be subsequently isolated to facilitate the detection of subtle variations and trends of their fluvial properties. Consequently, a Virtual Datum is the equivalent of having a marker bed crossing the stratigraphic succession of an outcrop at any desired position.

The advantages provided by a Virtual Datum proves to be especially useful in large and topographically complex outcrops that previously could not have been studied with such a high degree of 3D stratigraphic control.

## INTRODUCTION

Fluvial sandstones represent some of the commonest reservoir rocks, and a great deal of the hydrocarbon production worldwide is extracted from sediments that were deposited by ancient river systems. However, because this type of reservoir has a very complex distribution in the subsurface, accurate field studies to characterize outcrops as analogs of buried fluvial systems are needed.

The three-dimensional (3D) architecture of sandstone bodies is not only the most complex and unpredictable but also the most important fluvial attribute that must be taken into account when characterizing reservoirs located within ancient fluvial sedimentary successions (North and Prosser, 1993). As noted by Miall (1996), these deposits are difficult to map in detail because of the high lateral heterogeneity of their facies and the poor definition of individual beds in successions consisting of repeated channel and overbank units. This author also argued that the restricted lateral and vertical dimensions of the paleochannels and their associated sandy deposits, together with the nonlinear evolution of facies belts through time and space, hamper our understanding of the 3D architecture and distribution of petrophysical properties within these sedimentary systems.

Methods employed to study hydrocarbon reservoirs are mainly seismic surveys, well logs and cores, which lack sufficient spatial resolution to properly characterize the geometries and sedimentological properties of the discrete elements composing fluvial reservoirs (Li et al., 2012). To this end, a number of studies have been focused on the detailed characterization and modeling of outcropping analogs as good approximations for understanding the behavior and spatial arrangement of fluvial reservoirs (Willis and White, 2000; Martinius and Næss, 2005; Miall, 2006; Pranter et al., 2009; Li et al., 2012). However, most of the available outcrops are composed of 2D sections, and geological expertise is needed to design accurate 3D reconstructions to determine parameters such as channel sinuosity, connectivity and continuity (Pringle et al., 2006).

**Correlation uncertainty**

Strong stratigraphic control is required when working in fluvial outcrops in order to perform accurate 3D characterizations of the geometries and stratigraphic architecture of sandstone bodies. The high lateral and vertical heterogeneity of facies in fluvial environments causes the uncertainty of the correlations to increase with the number of sandstone bodies and the distance between them.

Li et al. (2012) made an experiment to quantify the relationship between the density of data and the accuracy of correlations. First, these authors established a base case performing a high-resolution stratigraphic analysis based on 58 sections of a 30 Km-wide Cretaceous fluvio-deltaic outcrop. Subsequently, they designed three different datasets with progressively fewer sections than the base case in order to compare the interpretations made for each dataset. The results showed how, in extreme cases, overcorrelation led to the identification of only 40% of the existing fluvial bodies, whose widths and thicknesses were exaggerated by about 400% (Li et al., 2012). These results indicate how inaccurate

74 correlations may result in very different stratigraphic frameworks, profoundly affecting the
75 sizes, geometries and connectivities of the reservoir facies during subsequent modeling.
76 Geologists working in the characterization of large fluvial outcrops have used
77 different methods to obtain a stratigraphic control over sedimentary successions, of which the
78 use of marker horizons provides the most accurate and reliable correlations. Typical marker
79 horizons are coal, paleosol or volcanoclastic levels, which are assumed to have been
80 generated at a specific time and can extend tens of kilometers along the surface of fluvial
81 systems (Miall, 1996). Similarly, the presence of major erosional surfaces (if flat) or of large
82 tabular sandstone bodies can also be used as good datums. Unfortunately, in many outcrops
83 the use of marker horizons is not possible because these either are absent or covered by debris
84 or vegetation. In such cases, the correlation criteria will be largely based on the identification
85 of similarities between the characteristics of the sandstone bodies (e.g., size, geometrical
86 proportions, internal architecture and elevation) and/or on the recognition of distinctive
87 sequential arrangements (e.g., amalgamated intervals, coarsening/thickening trends and
88 prograding/retrograding sequences). However, given that these methods are strongly
89 conditioned by subjective interpretations, the resulting correlations will continue to be
90 uncertain. Moreover, the degree of uncertainty increases when correlating between nearby
91 outcrops or between several outcrop faces that cannot be observed from the same location
92 because of topographical constraints (e.g., if they are located in parallel valleys or on
93 opposite slopes of the same hill), which rules out direct visual correlation or the use of
94 photomosaics.
95 **Background studies using TLS for characterizing geological outcrops**
96 In recent years, improvements in digital data collection techniques and processing
97 software have led to significant advances in the field of outcrop characterization (Pringle et
98 al., 2004; Enge et al., 2007; Jones et al., 2011). This evolution is based on the premise that

99 the greater the quantity, quality (accuracy) and speed of data collection, the better constrained
100 the deterministic models derived from them (McCaffrey et al., 2005; Buckley et al., 2008;
101 Jones et al., 2008; Faubel-Pérez et al., 2010). In this regard, Pringle et al. (2006) provide a
102 review of the different digital data collection methods, highlighting Terrestrial Laser
103 Scanning (TLS) as the preferred technique of geologists. TLS is based on lidar technology,
104 which although developed in the early 1960s, has only recently been incorporated into the
105 study of geological outcrops. Lidar typically uses the two-way travel time of a laser pulse to
106 determine the distance to a target as sonar uses sound waves or as radar uses radio waves, but
107 with a much higher resolution and accuracy. The word lidar has been commonly attributed to
108 the acronym for *li*ght *d*etection *a*nd *r*anging in the literature. However, according to the
109 Oxford English Dictionary and the first paper that refers to this technology (Ring, 1963), it is
110 a portmanteau word for *li*ght + ra*dar*.
111 The main advantages of TLS over the rest of digital data collection techniques are the
112 following: (1) very rapid collection of high amounts of 3D data (thousands of points per
113 second); (2) high resolution (few centimeters) and accuracy; (3) acquisition of information
114 about the scanned materials through the intensity of the returned pulse (Burton et al., 2011);
115 and (4) photorealistic 3D data visualization obviating the need to create a mesh from the
116 point cloud, avoiding thereby the generation of extra geometries (Kreylos et al., 2013).
117 In the last decade, TLS has been used to characterize geological outcrops with diverse
118 purposes. Examples include the following: study of dinosaur footprints (Bates et al., 2008);
119 characterization of folds, faults and fracture networks (Baker et al., 2008; Olariu et al., 2008;
120 Jones et al., 2009; Wilson et al., 2009; García-Sellés et al., 2011; Pearce et al., 2011; Wilson
121 et al., 2011); and geometrical depiction of carbonate platforms (Phelps and Kerans, 2007;
122 Verwer et al., 2009).

Regarding the study of channelized bodies, several works have been focused on the detailed description, characterization and modeling of sandstone bodies (Labourdette and Jones, 2007; Pranter et al., 2007; Faubel-Pérez et al., 2009; van Lanen et al., 2009; Pyles et al., 2010; Olariu et al., 2011; Olariu et al., 2012; Rittersbacher et al., 2014; Sahoo and Gani, 2015); performing flow simulations (Klise et al., 2009; Nichols et al., 2011); the study of the alluvial architecture (Labourdette, 2011; Hajek and Heller, 2012); and building of geocellular and seismic 3D models (Enge et al., 2007; Janson et al., 2007; Buckley et al., 2010; Faubel-Pérez et al., 2010; Pringle et al., 2010; Tomasso et al., 2010). In these works, TLS data were mainly employed to characterize the internal/external geometries and spatial arrangements of sandstone bodies, whereas correlations were carried out by merely recognizing in the DOM the sedimentary features that have been traditionally used for correlation (e.g., marker beds, extensive sandstone bodies, major erosional surfaces or characteristic architectural arrangements). However, we consider that these correlation procedures do not exploit all the possibilities that an exhaustive analysis of TLS data can offer.

The main aim of the present paper is to provide a new TLS-based methodology leading to the creation of a Virtual Datum that furnish the degree of stratigraphic control needed to perform highly accurate correlations at outcrop scale and help solve some of the issues regarding the characterization of the fluvial reservoirs mentioned above.

## OUTCROPS UNDER STUDY

Fluvial outcrops selected for testing the suitability of using a Virtual Datum as a correlation tool are located near Huesca, NE Spain (Fig. 1). Their sediments were deposited in the early Miocene by rivers that flowed through the Huesca Fluvial Fan (Hirst and Nichols, 1986; Hirst, 1991; Nichols and Hirst, 1998; Jones, 2004; Luzón, 2005; Fisher and Nichols, 2013). This fluvial system was developed adjacent to the northern boundary of the Ebro Foreland Basin under endorheic conditions (Puigdefàbregas and Souquet, 1986;

148 Puigdefàbregas et al., 1992; Barnolas and Gil-Peña, 2001), and have been classified as
149 pertaining to the Sariñena Fm. (Quirantes, 1969).
150 The closure of the connection between the Ebro Foreland Basin and the Atlantic
151 ocean during the Priabonian (Costa et al., 2010) marked the onset of a widespread deposition
152 of thick continental sequences throughout the basin, resulting in the development of a series
153 of large distributive fluvial systems (Hartley et al., 2010) spreading out from the surrounding
154 mountain ranges, e.g., Montsant, Guadalope-Matarranya, Caspe, Luna and Huesca (Allen et
155 al., 1983; Hirst, 1991; Puigdefábregas et al., 1991; Möhrig et al., 2000; Jones et al., 2001;
156 Luzón and González, 2003; Luzón, 2005; Nichols, 2005; Cuevas et al., 2007; Barrier et al.,
157 2010). The Huesca Fluvial Fan was the largest one, with a radius of about 60 Km, covering
158 an area of around 4500 $Km^2$ and presenting thicknesses exceeding 1000 m (Hirst and
159 Nichols, 1986; Hirst, 1991; Nichols and Hirst, 1998). This fluvial system evolved between
160 the late Oligocene and the lower Miocene (Luzón and González, 2003) adjacent to the
161 External Sierras, which were formed by the southward propagation of the South Pyrenean
162 Frontal Thrust (SPTF in Figure 1). Its sediments were sourced from the Pyrenean axial zones
163 and from the exhumed south Pyrenean piggy-back basins (Jupp et al., 1987; Vincent and
164 Elliott, 1997; Vincent, 2001; Yuste et al., 2004), and were transferred towards a perennial
165 lake located at the basin center (Cabrera and Sáez, 1987; Arenas and Pardo, 1999; Cabrera et
166 al., 2002; Cabrera et al., 2011) (Fig. 1).
167 The Huesca Fluvial Fan developed after the main phases of deformation in the
168 adjacent Pyrenees (Fisher and Nichols, 2013) in a context where the aggradation rates
169 exceeded those of basin subsidence (Nichols, 2004, 2007). This suggests that tectonic
170 controls did not play a significant role in the evolution of the system. Climatic controls can
171 also be ruled out because of the lack of clear cyclical sequential arrangements in the vertical
172 architecture of the available outcrops (Fisher and Nichols, 2013). Owing to the lack of

significant allogenic forcings, the evolution of the Huesca fluvial Fan was largely controlled by autogenic processes, especially by the major avulsions triggered by cycles of channel backfilling and plugging (Nichols, 2007; Fisher and Nichols, 2013; Ventra et al., 2014). The resulting fluvial architecture largely consists of isolated to amalgamated sandstone lenses and sheets surrounded by fine-grained floodplain sediments, which is the characteristic facies arrangement of labyrinthine-type reservoirs (Webber and van Geuns, 1990).

Montearagón and Piracés outcrops (Fig. 1) are located approximately 45 Km away from the estimated apex of the Huesca Fluvial Fan (Jupp et al., 1987) and have been interpreted as belonging to the medial part of this fluvial system (Hirst, 1991). Despite being about 16 km apart, they are assumed to be located in similar stratigraphic positions like most of the outcrops of fluvial fan deposits in the zone (Cuenca et al., 1992). This is due to a slightly tilted sedimentary succession (typically $<1.5^{o}$) and to the relatively smooth structural relief (<100 m) existing across the whole fan area. In the absence of chronological data for the Montearagón and Piracés outcrops, biostratigraphic and geochronological datings in the proximity suggest a lower Miocene age (Álvarez-Sierra et al., 1990; Odin et al., 1997).

The Montearagón outcrop is located adjacent to the Flúmen river, 5 Km NE of Huesca (Fig. 1). It is composed of two parallel and unconnected slopes of kilometric length (Montearagón in the south and Barranco Hondo in the north, Fig. 2A) that present a fluvial succession about 80 m thick. The Piracés outcrop is located in the surroundings of the village of the same name (Fig. 1), and comprises more than 6 Km of steep and continuous slopes of about 100 m. This outcrop can be subdivided into two sectors (Fig. 2B): an amphitheater opened towards the SE (located to the N of Piracés), and a NW-SE trending cliff facing SW (located to the NW of the same village).

The two outcrops present several cliffs oriented towards the SW and/or NE (Fig. 2), which together with main paleocurrents towards the W-SW (Friend et al., 1986; Friend et al.,

198 1989; Hirst, 1991) theoretically should provide numerous cross-sections of paleochannels.
199 However, they differ in three-dimensionality and physiographic complexity as well as in the
200 proportion and size of paleochannels (Hirst, 1991).

201 **Sedimentary facies**

202 Seven detailed stratigraphic logs (1:50 scale, more than 550 m in length, see location
203 in Figure 2) were measured in the Montearagón outcrop to characterize the facies and verify
204 the quality of the correlation results. Lithofacies described in Montearagón can be
205 extrapolated to Piracés since both outcrops are located at similar radial positions of the same
206 fluvial system (Fig. 1). Earlier studies carried out in the area (Friend et al., 1989; Hirst, 1991;
207 Donselaar and Schmidt, 2005; Luzón, 2005) and observations made during the different TLS
208 acquisition campaigns support this premise. Outcropping lithologies largely consist of fine to
209 medium-grained sandstones embedded in siltstones and mudstones with scarce occurrences
210 of centimeter-thick limestone levels (Fig. 3), and have been classified into channel-fill and
211 overbank facies

212 Channel-fill facies are mostly medium grained, although coarse sandstone and/or
213 pebbles are occasionally found forming basal lags, and typically exhibit a fining-upward
214 granulometric trend to fine and very fine sandstone at the top. Most paleochannels show flat
215 erosional basal surfaces that grade laterally to well-defined cut banks and are poorly incised
216 into older deposits owing to the characteristic aggradational trend that prevails in endorheic
217 basins (Nichols, 2004, 2007, 2012; Fisher and Nichols, 2013; Ventra et al., 2014). Trough
218 cross-bedded sedimentary structures are commonly present in the lower parts of the
219 paleochannels, whereas horizontally stratified and ripple cross-laminated fine sandstone
220 dominate their upper parts. Clay plugs, which are also common, are the product of the passive
221 infill of abandoned channels with sediments transported as suspended load during flooding
222 events. Paleochannels in the medial zone of the Huesca Fluvial Fan have been interpreted as

223 the deposits of braided, meandering and straight channels, which distally show a tendency to
224 reduce their dimensions and increase their lateral stability as a result of a decrease in stream
225 power (Hirst, 1991; Nichols and Fisher, 2007). In outcrop, sandstone beds stand out as steep
226 rock faces owing to the lower erodibility of this lithology with respect to the surrounding
227 fine-grained sediments. This contrast in erodibility is enhanced by a late-diagenetic calcite
228 cementation of sandstones (Donselaar and Schmidt, 2005).
229 Overbank facies are composed of variable amounts of sand, silt and clay-rich
230 sediments with an average content of carbonate of 30%, and were deposited from the
231 suspended load during floods (Nichols and Hirst, 1998). The coarsest overbank sediments are
232 found adjacent to the paleochannel margins in the form of levee deposits (Fig. 3, A). They
233 consist of inclined beds of alternating sandstone/mudstone that extend from tens to hundreds
234 of meters towards the floodplain, forming the characteristic channel "wings" (Fig. 3, B).
235 Crevasse splays consist of extensive sheets of fine sandstone that typically show thicknesses
236 exceeding one meter, non-erosive bases, coarsening-upwards sequences and a predominance
237 of planar and ripple laminations. The feeder channels of these crevasse splays are constituted
238 by small-scale ribbons (<1 m thick) of fine sandstone. The finest sediments, which were
239 deposited by decantation in the waning stages of floods, constitute the bulk of the floodplain
240 facies. Thin limestone levels occasionally occurring within the fine-grained intervals and the
241 top of sandstones are attributed to the precipitation of carbonate from ponded waters.
242 Evidence of pedogenic processes associated with incipient paleosol development is
243 found in the form of reddish decolorations, light yellow levels with versicolor mottlings
244 (usually associated with rhyzoliths), gray levels with iron nodules and carbonate and gypsum
245 concretions in the finest sediments. The development of these paleosol horizons has been
246 associated with periods of non-deposition since their degree of maturity increases with
247 distance from the active channels (Hamer et al., 2007a). Trace fossils are widely present in

both overbank and channel fill facies as rhyzoliths, burrows and ant/termite nests. These traces do not always reach the top of the sandstone beds, which in the case of the channel fills suggests a discontinuous water regime since the fauna could not have colonized the bed of the channels had these been continuously active.

Friend et al. (1986) proposed a classification for the sandstone-bodies of the Huesca Fluvial Fan, which was later applied regionally by Hirst (1991). This classification is based on the cross-sectional external geometry and on the internal architecture of the paleochannels. Further descriptions and interpretations of paleochannel types and their internal architectures can be found in Nichols and Hirst (1998), Donselaar and Schmidt (2005) and Luzón (2005).

## METHODOLOGY

### DOM design

TLS is a remote sensing technology that uses the orientation angles of emitted laser pulses and their traveled distance, which is mainly extrapolated by using their time-of-flight, to determine the relative coordinates of a target with respect to the scanning location (García-Sellés et al., 2011). The device records each returned pulse as a point with relative coordinates, two-way travel time and signal intensity, and gathers thousands of points per second with a resolution of a few centimeters (at distances of hundreds of meters). During subsequent processing stages, the resulting point clouds are textured with high-resolution photographs, merged in a single point cloud, and later georeferenced by means of GPS (Global Positioning System) data. The result is a Digital Outcrop Model (DOM) that is ready for inspection and interpretation in order to measure and quantify any property of geometrical nature, e.g., bedding attitudes, fracture orientations, distances, thicknesses, areas and volumes.

#### *Lidar data collection*

This study was carried out with an Ilris-3D TLS device from Optech. According to the manufacturer, it is capable of registering more than 2000 points per second at a maximum distance of 1200 m (assuming optimal atmospheric conditions and target reflectivities of at least 80%), reaching maximum range and positional accuracies at 100 m of, respectively, 7 mm and 8 mm.

Lichti (2004) established that positional resolution of a laser scanner (defined as the level of identifiable detail within a scanned point cloud) is governed by the sampling interval and the laser beamwidth, which in turn are dependent on the scanning distance. Accordingly, he proposed a new parameter termed EIFOV (Effective Instantaneous Field Of View), which establishes the maximum resolution that can be achieved at different distances with a certain device. In the present study, scanning distances to the outcrop surface were mainly between 150 m and 550 m, which in the case of the Ilris-3D results in EIFOV resolutions ranging from 4 cm to 10 cm.

The Ilris-3D has a built-in CMOS sensor to acquire a digital image associated with each scan. However, the poor quality and resolution of this sensor demanded the use of an external camera to achieve a satisfactory photorealistic effect. For this purpose, a Canon EOS 40D camera was assembled over the TLS device and calibrated to ensure an adequate fit between each point of the DOM and its corresponding pixel in the photograph. The calibration process was carried out at the Geological Survey of Denmark and Greenland (GEUS) using a theodolite-surveyed steel grid with 110 targets and a calibration software developed by the Technical University of Denmark.

Accurate georeferencing of the scans is necessary to obtain well-oriented measurements from the DOM. To this end, positioning data in UTM coordinates were acquired using a Topcon GB-1000 GPS with post-processing. The GPS receiver gathered data between 15 and 25 minutes at each scanning location. These measurements were later

297 derive-corrected using the GPS base station of the Escuela Politécnica Superior de Huesca. A
298 final resolution of a few centimeters (of the same order as that of the TLS data) was reached
299 in this way.
300 Data was acquired from 39 scanning stations, 18 in Montearagón and 21 in Piracés
301 (depicted with red dots in Figure 2). At each scanning station, the entire surface of the
302 outcrop located within the TLS detection range was captured by means of a series of
303 consecutive scans, which were acquired with an overlap of about 25% in order to enable their
304 correct alignment and merging during the subsequent processing stages. It should be noted
305 that, before acquisition, a proper planning to obtain the maximum coverage by using the
306 minimum number of scanning stations will optimize time and resources, especially in
307 outcrops of such size and topographical complexity as Piracés.
308 The digital dataset obtained consists of more than 140 million of points distributed in
309 149 individual scans (56 from Montearagón and 93 from Piracés) and the high-resolution
310 photographs and positioning data associated with each scan and scanning station,
311 respectively.
312 ***Processing***
313 Alignment of the individual scans was carried out with the IMAlign module of
314 PolyWorks®, which uses the Iterative Closest Point method (Chen and Medioni, 1992) to
315 obtain the best fit between the overlapped areas of two scans. First, the scans acquired from
316 the same place were aligned, which resulted in as many individual point clouds as scanning
317 stations. Subsequently, those point clouds with overlapped areas were aligned again, which
318 should ideally provide a single point cloud of the entire outcrop if all the captured surfaces
319 were interconnected. This was not the case, and some of the point clouds remained
320 unconnected after alignment between the scanning stations. Under these circumstances, the
321 assembly of the whole DOM is completed during the subsequent georeferencing phase.

Since the alignment process described above was performed in a 3D digital environment where the coordinates are relative to the TLS device, GPS coordinates measured at each scanning station were needed for georeferencing the DOM. To this end, PolyWorks® enables us to automatically extract the location of the scanning device for each scan and represents it as a point. If the process of alignment was correct, the location points of the scanning device for scans acquired from the same place should coincide. However, in practice they constituted narrow clusters of points, with the result that the UTM coordinates of each scanning location were finally assigned to the mass center of their corresponding cluster.

The result of this processing was a georeferenced DOM ready for interpretation and from which extraction of geographically oriented features is possible.

**Extraction of a Virtual Datum**

The sequence of steps and verifications that must be followed to obtain a proper Virtual Datum from the analysis of a DOM is depicted as a flow diagram in Figure 4. All the processes described in this flow diagram were carried out with the IMInspect module of PolyWorks®, which offers a series of tools enabling visualization, edition, interpretation and analysis of large lidar datasets.

The DOM was interpreted respecting the original point data instead of using a gridded mesh or a filtered point cloud. This ensures that no information is lost and prevents the creation of extra geometries or artifacts. Further arguments and discussions regarding the benefits of using raw point-based vs. gridded datasets can be found in Buckley et al. (2008) and Kreylos et al. (2013).

***Prior considerations***

The idea of using a planar surface as a Virtual Datum is based on the hypothesis that the depositional paleosurface of the fluvial fan can be represented by a plane at outcrop scale.

Thus, since the surface of a fluvial system constitutes an isochronous level, the plane that represents its overall geometry can be used to identify the materials that coexisted over the local fan surface (i.e., as a reference surface for correlations).

The DOM of an adequate fluvial outcrop can be used to indirectly derive the geometry of the original depositional surface. To this end, several stratigraphic horizons with its same geometry as that of the depositional paleosurface must be digitized to infer the orientation of the planar surfaces that best fit them. Paleosol levels are very suitable for this purpose for the same reason that they are used as datums to perform correlations, i.e. they develop in the surface of the fluvial system as continuous horizons with large lateral extensions. However, paleosols are not abundant or well developed in the studied outcrops, and when present they are not easy to track in the DOM since they are usually covered by debris or vegetation. Alternatively, the upper boundaries of the sandstone bodies (i.e., paleochannel fills) were selected for digitizing. These bodies are numerous in the outcrops and crop out forming laterally extensive exposures that are easily detected and may be traced in the DOM along hundreds of meters. As a result, they are the most suitable sedimentary bodies from which to calculate a Virtual Datum. Although they do not provide an approximation that is as accurate as paleosols or other marker beds, it may be assumed that the tops of the channel fills were deposited in the same way as the surrounding floodplain (Fig. 5). The reason for this is that under aggradational conditions (such as those that prevailed in the endorheic Ebro Basin), fluvial systems and hence fluvial courses tend to maintain stable slopes through time (Nichols, 2012; Fisher and Nichols, 2013; Ventra et al., 2014).

The outcrop should have a high degree of three-dimensionality to ensure satisfactory results. This is because the larger the roughness of the outcrop surface, the better constrained the geometrical reconstruction of a specific horizon from its intersection with the topography.

Otherwise, in a purely 2D outcrop like a vertical cliff or a road cut, digitization of a flat stratigraphic horizon will result in a straight line, which could be contained by several different planes.

However, the main limitation of the method is that it is only applicable to fluvial outcrops where the sedimentary succession is undeformed or homogeneously tilted. This excludes the outcrops where post-depositional tectonic processes (e.g., folding and faulting) have modified the original depositional surface in such a way that it can no longer be represented locally by a plane.

***Digitization***

Instead of following the exact shape of the tops of the sandstone bodies (red line in Figure 6), polylines must be digitized to depict their flat upper envelopes (i.e., a planar surface covering the external shape; green line in Figure 6). This is because digitization is focused on calculating the plane that best fits the top of the sandstone bodies at the scale of the entire paleochannel/paleochannel belt, which correspond to a $5^{th}/6^{th}$ order bounding surface of Miall (1988) (Table 1) or to 5a/6 bounding surface of DeCelles et al. (1991). Thus, the irregularities produced by sub-channel scale ($<5^{th}$ order) forms and processes (e.g., channel bars, levees, clay plugs and erosional events; Fig. 6) can be ignored, which leads to the calculation of planes with better adjustments to their parent polylines.

PolyWorks®, like most of the commercially available CAD software packages, offers two projection modes to display 3D data (reality) in 2D (screen): perspective and orthogonal. A perspective projection represents the objects in the same way that a human eye sees the scene in reality, with distant objects appearing smaller than closer ones. By contrast, orthogonal (or orthographic) projection ignores this effect, allowing the creation of scaled drawings where angles, sizes and heights remain unaffected by distance (Fig. 7). The use of an orthogonal projection for digitizing is highly recommended because it enables us to

397 display the outcropping geobodies without perspective distortions. Its utility can be readily
398 demonstrated when we consider the hypothetical case of working with a DOM composed of
399 horizontal strata cropping out discontinuously across any topographical context. With an
400 orthogonal projection, and if only the Z axis is used for rotations (untilted views), all the
401 bedding surfaces will be displayed as straight lines regardless of the angle of view or the
402 distance from the observer. However, with a perspective projection this only occurs when the
403 surface is exactly at the same height as the observer (blue line in Figure 7A), while the rest of
404 flat surfaces will be displayed as sinuous lines, hindering a proper digitization and the
405 subsequent correlation process.

406 Once the tops of sandstone bodies are digitized, the next step involves the calculation
407 of the planes that best fit the digitized polylines. This was accomplished in the present study
408 by using an in-house developed macro that is based on analyzing the moment of inertia of a
409 point set (Woodcock, 1977; Fernández, 2005; García-Sellés et al., 2011). Input data were
410 obtained by selecting the closest points to the considered polyline (those located at a distance
411 of less than 10 cm), after which the macro was able to calculate the orientation and position
412 of the plane that best fits them, finally drawing it within the DOM (Fig. 8).

413 The quality of the adjusted plane is assessed by two parameters (Fernández, 2005):
414 coplanarity (M) and collinearity (K). Coplanarity refers to the degree of fit between the plane
415 and the points from which it was calculated with higher values indicating better adjustments.
416 Collinearity is derived from the quantification of the 3D distribution degree of these points,
417 providing information about the reliability of the plane, with K=1 indicating a linear
418 distribution and progressively smaller values denoting better distributed point sets. Given
419 these considerations, the higher the M and the lower the K, the better the quality and
420 representativeness of a plane. Acceptable values of $M>4$ and $K<0.8$ were suggested by

Fernández (2005) when working with the intersection between geological surfaces and the topography.

After this first phase of interpretation, several tens to hundreds of lines together with their associated planes were obtained. The quality of these planes (acceptable M and K values) must be revised to ensure that the tops they represent were properly digitized. Should this not be the case, the original polylines must be improved in order to obtain better adjustments (Fig. 4).

***Initial correlations***

The next phase focuses on the identification and correlation of all the sandstone bodies that are located in the same stratigraphic horizon. This process is undertaken by a trial and error method that adopts a progressive approach towards a single plane of the upper boundaries of all the contemporary sedimentary units.

The preliminary correlations should be made by considering a large and laterally continuous sandstone body from which various exposures can be identified. The use of several distant polylines will enable us to calculate a plane from a better three-dimensionally distributed point set, thus ensuring low K values (high reliabilities). Subsequently, the geometrical relationships of this plane with respect to the remaining outcropping elements must be verified in order to establish whether it should be regarded as valid for further testing or discarded. The simplest way to do this is to expand the plane along the DOM (Fig. 4), but the fact that the data are concealed behind the plane hampers a proper evaluation of the plane-DOM intersection (Fig. 8B). This problem was solved by selecting the points located within a certain range from the plane, which resulted in a line of red points that enabled us to remove the plane (Fig. 8C).

Two variables must be considered to determine whether a plane is suitable for correlation: coincidence with other tops and its relationship with respect to the other

446 stratigraphic horizons (parallel or oblique). Of these variables, the oblique cutting of any
447 stratigraphic level (e.g., sandstone bodies, limestone levels, paleosols and ash layers) is the
448 most obvious reason for rejecting a plane, and is therefore the key aspect that must be
449 verified (Fig. 9). In other words, a plane will be taken into account only if it maintains a
450 parallel relationship with all the stratigraphic horizons along the entire outcrop. Henceforth,
451 all the planes regarded as valid must fulfill this requirement.

452 There are other indicators providing information about the degree of reliability of the
453 calculated correlation planes. For instance, the situation in which a valid plane coincides both
454 with the tops and the internal scours of other sandstone bodies (red line in Figure 10F) is the
455 most favorable one since this strongly suggests that the plane denotes a significant
456 stratigraphic level. However, if the opposite is the case (i.e., when it does not match any top
457 or internal scour), the suitability of the plane will continue to be in doubt. In such cases, the
458 performance of correlation tests in a sandstone-richest stratigraphic level will be the best
459 option as this should provide more constrained and reliable results.

460 When a valid plane shows new coincidences with the upper boundaries of other
461 sandstone bodies, it must be calculated again incorporating their polylines as additional input
462 data. This will result in a new plane with an orientation very similar to the original one and a
463 better K (reliability). Again, this plane could present new coincidences with other tops not
464 previously considered, entailing a new recalculation. This process should be repeated
465 successively until a final correlation plane is calculated taking into account all the possible
466 interrelated sandstone bodies of the studied stratigraphic level.

467 Locating polylines that show small-scale deviations with respect to the plane they
468 defined is frequent, especially if the latter shows a relatively low M (coplanarity). This does
469 not always imply that these tops were miscorrelated since sandstone bodies usually lack a
470 sharp and planar upper limit. As noted above, and shown in Figure 6, this may be attributed

to irregularities due to bedforms, to subsequent erosive processes or to the presence of debris in the upper parts of the sandstone levels. One way to deal with this issue is to modify the trajectory of the polylines by adapting them to the plane-DOM intersection, which ensures better coplanarities during subsequent recalculations of the plane defined by them. However, this practice is only recommended when dealing with planes whose accuracy and reliability have been tested in various stratigraphic levels, and in circumstances were the modified polylines continue to represent the sandstone tops. Either way, care should be taken during early phases of correlation to avoid falling into a circular reasoning in which better adjustments are achieved because the polylines are adapted to the plane rather than the opposite.

***Virtual datum establishment***

The process described above must be repeated for several significant stratigraphic levels, preferably the ones that are more channel-prone, in order to determine whether the orientation of the correlation planes calculated from them is similar or not.

In the case of a sedimentary succession with no angular unconformities, which means that all their materials remain undeformed or have undergone post-depositional tilting (i.e., tilted to the same degree), the orientation of all the correlation planes should ideally be the same. Then, one Virtual Datum can be used for correlation within the entire outcrop. By contrast, if the outcrop presents angular unconformities (suggesting a synsedimentary tilting) the same plane will not be valid for correlation within the entire sedimentary succession and more than one Virtual Datum will be necessary, each one being applicable only within the stratigraphic interval from which it was calculated.

A Virtual Datum must be continuously supervised taking into account that it will continue to be applicable to the sedimentary succession as long as a parallel relationship with all the stratigraphic surfaces is maintained.

## RESULTS AND PRACTICAL APPLICATIONS

A Virtual Datum was calculated for each of the two outcrops under study after applying the process described above. The Virtual Datum, and hence the bedding attitude presents a maximum dip of 1.22° towards 236° in the Montearagón outcrop, and a maximum dip of 1.54° towards 233° in the Piracés outcrop. In both cases, this digital tool for stratigraphic subdivision revealed its ability to correlate the sandstone exposures pertaining to the same paleochannel and their laterally associated overbank deposits (Figs. 9 and 10).

The accurate correlations provided by a Virtual Datum may be used as the base to design accurate 3D deterministic reconstructions of individual paleochannels/paleochannel belts and their associated overbank deposits in a way similar to that of Sahoo and Gani (2015). Increased certainty in the correlation of elements despite the fact that they are hundreds of meters apart or located in adjacent hills (Fig. 10) minimizes the number of cases where several exposures are erroneously regarded as the same sandstone body or vice versa. This avoids erroneous geometrical reconstructions of the paleochannels and incorrect assessments of the connectivity between sandstone bodies in subsequent stages of outcrop modeling. The same reasoning may be applied to the sandy overbank deposits, the miscorrelation of which will have an even greater impact on the model if laterally connected to the paleochannels.

In addition to being strictly a correlation tool between individual elements, the use of a Virtual Datum offers the possibility of identifying along an outcrop (or along various adjacent ones) the materials that coexisted on the fan surface. Thus, it can be used to isolate specific stratigraphic intervals from the remaining sedimentary succession, facilitating a rapid and accurate subdivision of the DOM into slices with a stratigraphic significance. This is shown with an example of each of the outcrops in Figure 11, where the stratigraphic slices were obtained by placing the Virtual Datum on the top of a large paleochannel and by

selecting all the points located below the plane up to a distance equal to the maximum thickness observed for the sandstone body. Stratigraphic intervals can later be characterized separately in order to facilitate the detection of subtle spatial variations and vertical trends of several fluvial properties both within and between stratigraphic slices (e.g., sandstone proportion, channel size and typology, connectivity of reservoir facies, amalgamation index and geometry of the overbank deposits). This accurate 3D stratigraphic control can also be used as the base to perform a series of deterministic facies reconstructions of several intervals to evaluate the paleogeographic evolution in the zone.

There is also the possibility of digitizing the path of the stratigraphic logs in the DOM, which results in their automatic georeferencing and enables us to correct the thicknesses that were measured in the field by means of Jacob's staff (Fig. 3). The process of correction of the stratigraphic logs starts with the identification in the DOM of the sandstone bodies that are represented in them. Thereafter, the distance between their lower/upper limits and the point where the log started to be recorded is measured taking into account the dipping attitude of the sedimentary succession (provided by the Virtual Datum) to obtain true stratigraphic thicknesses. In the case of the studied outcrops, the regional dip is so close to horizontal that the measured vertical thicknesses are practically the same as the stratigraphic ones. The seven stratigraphic logs that were measured in Montearagón (Fig. 2A) were selected to test this method. After correction, differences ranging from 1.58% to 5.06% between the measured and real sedimentary thicknesses were found, with an average thickness underestimation of 2.95% (see Table 2). The possible reasons behind this general underestimation of the real thicknesses will be discussed below.

The availability of georeferenced and corrected stratigraphic logs together with the certainty in the correlation provided by the use of a Virtual Datum enabled us to design a highly accurate correlation panel (Fig. 12). To this end, the logs were placed in accordance

with the real distance existing between them in a way similar to that of van Lanen et al. (2009) for the Wolfville Fm., and their relative vertical position was set using the Virtual Datum, which enabled us to restore the tilting of the series to horizontal. Furthermore, the geometries and thicknesses of the sandstone bodies between stratigraphic logs were drawn with the assistance of the continuous quantitative and qualitative information provided by the DOM. Consequently, the resulting correlation panel faithfully reflects the real dimensions, proportions and lateral/vertical relationships of the different facies, placing especial emphasis on the sandstone bodies.

The high degree of 3D stratigraphic control provided by a Virtual Datum proves to be very useful for extracting the accurate and realistic input data that are needed to perform a proper modeling as a reservoir analog from the DOM of fluvial outcrops, especially from the largest and most topographically complex ones. Furthermore, the advantages derived from its use can contribute to a better understanding of the driving mechanisms and processes that influence the evolution of fluvial systems.

## DISCUSSION

Geologists have used several methods and approaches to achieve proper body-to-body correlations and stratigraphic subdivisions in fluvial outcrops. These methods include the use of marker horizons (e.g., coal beds, volcanic ash layers and distinctive paleosols), comparison between the characteristics of the sandstone bodies (e.g., height in the outcrop, location inside sequential arrangements and detection of internal/external architectural similarities) as well as line drawings on photomosaics. Of these methods, only those based on distinctive and laterally extensive marker horizons provide accurate correlations. Nevertheless, most outcrops lack such sedimentary features owing to their low preservation potential inside active fluvial environments. Even if these marker horizons are present they rarely crop out continuously and are seldom located in the desired position. The other methods are

571 conditioned to a greater or lesser extent (depending on the quality, depositional architecture
572 and structural setting of the outcrop) by the subjectivity associated with any interpretation.
573 This means that different geologists studying the same area could end up establishing
574 different correlations using these methods, with a level of uncertainty that will increase in
575 proportion to the distance of correlation.

576 To overcome these difficulties, reliable correlations in outcrops of the Huesca Fluvial
577 Fan were performed using a Virtual Datum obtained by an exhaustive geometrical analysis of
578 their DOMs. The Virtual Datum consists of a plane that seeks to represent the average
579 geometry of the local fan surface at the time of sedimentation, which implies that its use will
580 be restricted to outcrops where the depositional paleosurface can be simplified with a plane.
581 This requirement is met in the two studied outcrops since it was possible to calculate a
582 Virtual Datum that fit all the stratigraphic levels without crosscutting relationships anywhere.
583 Such a parallel relationship with all the horizons of an outcrop can only be achieved if the
584 Virtual Datum represents the original depositional surface of the sedimentary system.

585 The upper boundaries of the sandstone bodies were used to calculate the Virtual
586 Datum for two reasons: (1) since they protrude from the outcrop surface, they are the most
587 easily recognizable sedimentary features that provide an approximation to the original
588 depositional paleosurface; and (2), exposures of laterally extensive sandstone levels (several
589 hundreds of meters wide) are very common, allowing the extraction of well-constrained
590 planes. This approach is similar to that used by Pyles et al. (2010) for the DOM of a
591 submarine channel complex, where these authors digitized the top of a clay plug of a
592 paleochannel to establish a datum ("paleohorizontal surface") in order to restore the
593 displacement of a normal fault.

594 The same procedure could have been carried out by identifying and digitizing
595 paleosol horizons, as they probably represent the best approximation to the paleosurface of

596 the fluvial fan. Unfortunately, paleosols are not well developed in the studied outcrops
597 (Nichols and Hirst, 1998; Hamer et al., 2007b), and when present they do not generate
598 prominent features, often remaining buried under debris or covered by vegetation. Thus, the
599 scarce paleosol exposures found in the outcrops are not laterally continuous enough to allow
600 us to calculate well-constrained planes from them.
601 Alternatively, paleochannel exposures were used to calculate Virtual Datums given
602 that the upper surfaces of the preserved sandstone bodies mimic the slope of the fan surface
603 (Fig. 5). This is the case at least in aggradational settings, where a constant rise of the base
604 level inhibits the development of major episodes of river incision (Nichols, 2012; Ventra et
605 al., 2014), avoiding significant increases in the gradient of the river profiles with respect to
606 the fluvial system surface. Furthermore, the progressive rise of the base level typical of
607 endorheic basins not only determines a mainly constant topographic gradient of the
608 depositional systems through time (which is also applicable to the profiles of the fluvial
609 courses) but also a general layer-cake stratigraphic architecture (Nichols, 2012; Fisher and
610 Nichols, 2013; Ventra et al., 2014). Climatically driven fluctuations in the level of the lake
611 located in the basin center may cause modifications in the profiles of fluvial systems since the
612 lake constitutes the base level of the basin. However, in such basins where the lake is very
613 shallow and the gradient of the lake floor is very low, as in the Ebro Basin, the changes in the
614 lake level have little impact on the fluvial systems (Nichols, 2012; Fisher and Nichols, 2013).
615 Another result of the absence of major phases of fluvial incision in aggradational settings is
616 that isochronous surfaces can be laterally extended through most of the considered lobe of the
617 fluvial system because they are rarely truncated by younger deposits. This allows us to
618 correlate across long distances using the geometry of the depositional surface. Therefore, the
619 aggradational conditions expected within endorheic basins enable us to use the paleochannel

deposits to infer the average orientation of the depositional paleosurface, facilitating the calculation of a Virtual Datum.

Like most of the geological surfaces, the sandstone tops are not strictly sharp and planar, and local-scale roughness is commonly observed (Figs. 6A and 6B). However, these irregularities are negligible when working at channel and channel belt scales so that the upper boundaries of significant sandstone bodies can be reduced to a flat upper envelope (Fig. 6C) that represents the overall attitude of the original depositional paleosurface (Fig. 5). Subsequent post-depositional deformations of the stratigraphic succession involve the modification of this primary surface, but in cases where the deformation is only related to a regional tilting, the plane-based correlations will still maintain their inherent stratigraphic significance.

As for the benefits arising from the use of a Virtual Datum, the ability to easily subdivide the entire sedimentary succession of an outcrop into stratigraphic slices simply by placing it at different altitudes provides an exceptional degree of control over the spatial distribution and temporal evolution of sedimentation. A comprehensive analysis of these stratigraphic intervals will facilitate the design of depositional models, offering greater insight into the evolution of the fluvial system and into its controlling mechanisms. Moreover, this high degree of stratigraphic control has deep implications for the modeling of outcrops as reservoir analogs. For example, the possibility of isolating a certain stratigraphic interval from the rest of the sedimentary succession facilitates the task of performing accurate deterministic reconstructions of the geometry and internal architecture of a given paleochannel and its related overbank deposits (Sahoo and Gani, 2015). Thereafter, these reconstructions will be used as input data to perform accurate object-based simulations. The availability of a precise stratigraphic subdivision also facilitates the detection of subtle spatial variations and trends concerning several properties (e.g., fluvial style, facies proportion, net-

to-gross ratio, grain size, porosity and distribution of lithofacies) within and between stratigraphic intervals. This is fundamental to obtaining the 3D variograms that are needed as input data to constrain the modeling.

A Virtual Datum will be applicable wherever a parallel relationship with the stratigraphic succession is maintained. This means that the use of a Virtual Datum calculated from one outcrop can be extended towards adjacent outcrops as long as no intersections with their stratigraphic horizons are found.

As for the quality of the sedimentological data acquired in the field with Jacob's staff, a DOM-based correction of the stratigraphic logs avoids biased estimations of facies proportions caused by their over/underestimation during the measurement process. This will improve subsequent reservoir models since stratigraphic logs are commonly used in the form of pseudowells as hard data to constrain modeling. After the correction of the stratigraphic logs that were measured in Montearagón, a general underestimation of the stratigraphic thicknesses was observed. As shown in Table 2, several factors that may have influenced the measurement process were considered, but no clear relationships were established. However, a comprehensive analysis of the distribution of errors within each stratigraphic log revealed that major measurement errors were mainly linked to moments when lateral displacements were required owing to the presence of thick sandstone bodies forming vertical cliffs of several meters. In order to facilitate lateral along-strike displacements, these were mainly performed on top of sandstone beds since they are thought to have a planar geometry and be isochronous along their extension. As pointed out above, this is not always the case, and the small-scale topography created by bedforms and erosional scours led to the errors of decimetric to metric order that have been found to be associated with the lateral displacements over sandstone tops (Fig. 6). Thus, stratigraphic logs that intersect a larger

669 number of thick sandstone bodies are more prone to present measuring biases than those that
670 do not require many lateral displacements.
671 The reasons behind the overall underestimation of the total thickness observed in all
672 the logs are less significant given that they are always produced in the same direction
673 (subtraction of total thickness in this case), suggesting that they are probably related to
674 subjective and/or technical systematic biases. For example, faults in the construction of
675 Jacob's staff, a geologist's tendency to add a few centimeters when performing visual
676 projections or an imprecise calibration of the bedding attitude can explain these systematic
677 errors. Anyway, here we note that the level of accuracy achieved by Jacob's staff
678 measurements is surprisingly high given the simplicity of the measuring tool and method, and
679 that it is suitable for most of the classic applications of the stratigraphic logs.
680 The use of the Virtual Datum can be extended to the DOM of any outcrop composed
681 of materials that were deposited in aggradational settings by a sedimentary system whose
682 original depositional surface is capable of being represented by a plane at outcrop scale.
683 Another requirement is that the sedimentary succession remains undeformed or
684 homogeneously tilted. As is well known from modern and ancient examples, the mechanisms
685 and processes driving the evolution of fluvial systems generally tend to form relatively flat
686 and continuous depositional surfaces. Therefore, outcrops whose materials were deposited by
687 rivers within endorheic basins are regarded as suitable for using a Virtual Datum. Other
688 sedimentary environments that tend to configure flat and extensive depositional surfaces
689 include non-marginal zones of lacustrine systems, delta plains (topsets) of deltaic systems
690 and submarine fans (turbidites). Nevertheless, further tests in such sedimentary outcrops are
691 necessary to justify the use of a Virtual Datum in them, bearing in mind that the major
692 incisions triggered by falls in the base level can disrupt the lateral continuity of the
693 isochronous stratigraphic surfaces.

To date, outcrops belonging to the Huesca Fluvial Fan have been studied individually ignoring their relative stratigraphic positions despite the fact that some authors have assumed that they are located inside the same stratigraphic level (Hirst, 1991; Donselaar and Schmidt, 2005). However, such unconfirmed assumptions may lead to miscorrelations and, hence, to misleading reconstructions of the fan paleogeography and facies distribution. For this reason, future work will be focused on the development of a methodology using Virtual Datums to correlate distant outcrops and deduce their relative positions inside the entire fluvial sequence. Our intention is to proceed in a way similar to that of structural geologists when characterizing folds and faults by establishing several dip domains from dip data measured in the field (Wise, 1992; Fernández et al., 2004; Carrera et al., 2009), but using the dips provided by Virtual Datums. We trust that further methodological development starting from the bases established herein will help to shed light on this issue.

## CONCLUDING REMARKS

A new TLS-based methodology to calculate a Virtual Datum that facilitates characterization of suitable sedimentary outcrops is presented. This tool consists in a plane that tries to mimic the geometry of the depositional paleosurface of the sedimentary system. It is obtained from the systematic reconstruction and analysis of the planes that best fit the upper boundaries of the sandstone bodies existing in a DOM. The procedure to calculate a proper Virtual Datum is described above and is schematized as a simple flow diagram in Figure 4.

The idea of using a planar surface as a correlation tool is based on the hypothesis that the original depositional surface of the sedimentary system can be represented by a plane at outcrop scale. This requirement was met in the two studied outcrops of the Huesca Fluvial Fan because a single Virtual Datum managed to subdivide their entire stratigraphic

718 succession without crossing any stratigraphic horizon, which can be achieved only if the
719 working hypothesis is valid.
720 Given the nature of this correlation tool, the applicability of a Virtual Datum will be
721 restricted to DOMs of outcrops whose materials were deposited over a locally flat surface and
722 in which the original depositional surface maintains its ability to be represented by a plane.
723 This includes the outcrops showing sedimentary successions that remain undeformed or are
724 homogeneously tilted, and excludes those presenting folds and/or faults.
725 The use of this digital tool provides a high degree of stratigraphic control inside the
726 DOM of suitable outcrops regardless of topographical complexities or limitations, thereby
727 facilitating extremely accurate correlations. The method is especially useful when dealing
728 with large-scale outcrops (of kilometric order) made up of several faces that are unconnected
729 or located on opposite sides of a hill, or when correlating through neighboring outcrops that
730 are hundreds of meters apart (i.e., when the inspection of the entire outcrop at the same time
731 is not possible). Under these circumstances, and especially in the absence of clear marker
732 beds, the use of a Virtual Datum emerges as the most suitable way to build a proper
733 stratigraphic framework taking into account all the available information.
734 Once a Virtual Datum is established for an outcrop, it can be placed on top of any
735 particular sandstone body to achieve an immediate identification of all its available exposures
736 even if separated by distances exceeding one kilometer. Thus, this tool allows us to identify
737 the exposures that belong to the same paleochannel or paleochannel belt, considerably
738 simplifying its subsequent 3D geometrical reconstruction and the analysis of its spatial
739 relationships concerning the remaining outcropping elements. Moreover, since the TLS is a
740 remote sensing technology the outcrop can be studied as a whole, the only limitations being
741 the sensor range and the availability of scanning locations with proper perspectives towards
742 the surfaces to be studied.

A Virtual Datum can also subdivide the entire outcrop into the desired stratigraphic slices without the need for additional criteria by only moving it vertically to a specific position and verifying its intersection with the DOM. Consequently, a Virtual Datum is the equivalent of having a marker bed crossing the entire stratigraphic succession in the desired position. Such a degree of stratigraphic control is very helpful to detect vertical variations and trends of properties (e.g., facies proportions, paleochannel size and type, depositional architecture).

In view of its numerous benefits, especially in large and topographically complex outcrops that lack suitable marker horizons, a Virtual Datum proves to be useful in building good models of reservoir analogs and in improving our understanding of the factors and mechanisms that influence the evolution of sedimentary systems.

## ACKNOWLEDGMENTS

This work was funded by the Spanish Government through the project MODELGEO (CGL2010-15294) and a FPI grant. We are indebted to David García for his work during the TLS acquisition campaigns and for showing us how to build a DOM. Thanks are due to Eduard Albert, Luís Valero and Pau Arbués for their assistance in the field and for the valuable geological discussions.

## REFERENCES CITED

Álvarez-Sierra, M. A., Daams, R., Lacomba, J. L., López-Martínez, N., van der Meulen, A. J., Sesé, C., and de Visser, J., 1990, Palaeontology and biostratigraphy (micromammals) of the continental Oligocene-Miocene deposits of the north-central Ebro Basin (Huesca, Spain): Scripta Geologica, v. 94, p. 1-77.

Allen, P. A., Cabrera, L., Colombo, F., and Matter, A., 1983, Variations in fluvial style on the Eocene-Oligocene alluvial fan of the Scala Dei Group, SE Ebro Basin, Spain: Journal of the Geological Society, v. 140, no. 1, p. 133.

Arenas, C., and Pardo, G., 1999, Latest Oligocene–Late Miocene lacustrine systems of the north-central part of the Ebro Basin (Spain): sedimentary facies model and palaeogeographic synthesis: Palaeogeography, Palaeoclimatology, Palaeoecology, v. 151, no. 1-3, p. 127-148.

Baker, B. R., Gessner, K., Holden, E. J., and Squelch, A. P., 2008, Automatic detection of anisotropic features on rock surfaces: Geosphere, v. 4, no. 2, p. 418-428.

774 Barnolas, A., and Gil-Peña, I., 2001, Ejemplos de relleno sedimentario multiepisódico en una
775 cuenca de antepaís fragmentada: La Cuenca Surpirenaica: Boletín Geológico y
776 Minero, v. 112, no. 3, p. 17-38.
777 Barrier, L., Proust, J. L., Nalpas, T., Robin, C., and Guillocheau, F., 2010, Control of Alluvial
778 Sedimentation at Foreland-Basin Active Margins: A Case Study from the
779 Northeastern Ebro Basin (Southeastern Pyrenees, Spain): Journal of Sedimentary
780 Research, v. 80, no. 8, p. 728-749.
781 Bates, K. T., Rarity, F., Manning, P. L., Hodgetts, D., Vila, B., Oms, O., Galobart, A., and
782 Gawthorpe, R. L., 2008, High-resolution LiDAR and photogrammetric survey of the
783 Fumanya dinosaur tracksites (Catalonia): implications for the conservation and
784 interpretation of geological heritage sites: Journal of the Geological Society, v. 165,
785 no. 1, p. 115-127.
786 Buckley, S. J., Enge, H. D., Carlsson, C., and Howell, J. A., 2010, Terrestrial laser scanning
787 for use in virtual outcrop geology: The Photogrammetric Record, v. 25, no. 131, p.
788 225-239.
789 Buckley, S. J., Howell, J. A., Enge, H. D., and Kurz, T. H., 2008, Terrestrial laser scanning in
790 geology: data acquisition, processing and accuracy considerations: Journal of the
791 Geological Society, v. 165, no. 3, p. 625-638.
792 Burton, D., Dunlap, D. B., Wood, L. J., and Flaig, P. P., 2011, Lidar Intensity as a Remote
793 Sensor of Rock Properties: Journal of Sedimentary Research, v. 81, no. 5, p. 339-347.
794 Cabrera, L., Arbués, P., Cuevas, J. L., Garcés, M., López-Blanco, M., Marzo, M., and Valero,
795 L., 2011, Integrated analysis of a marine to continental transition in an evolving
796 foreland: advanced case studies in the eastern Ebro Basin (Eocene-Early Miocene), *in*
797 Arenas, C., Pomar, L., and Colombo, F., eds., Geo-Guías, 7, Pre-Meeting Field Trips
798 Guidebook, 28th IAS Meeting: Zaragoza, Sociedad Geológica de España, p. 151-198.
799 Cabrera, L., Cabrera, M., Gorchs, R., and de las Heras, F. X. C., 2002, Lacustrine basin
800 dynamics and organosulphur compound origin in a carbonate-rich lacustrine system
801 (Late Oligocene Mequinenza Formation, SE Ebro Basin, NE Spain): Sedimentary
802 Geology, v. 148, no. 1-2, p. 289-317.
803 Cabrera, L., and Sáez, A., 1987, Coal deposition in carbonate-rich shallow lacustrine
804 systems: the Calaf and Mequinenza sequences (Oligocene, eastern Ebro Basin, NE
805 Spain): Journal of the Geological Society, v. 144, no. 3, p. 451-461.
806 Carrera, N., Muñoz, J. A., and Roca, E., 2009, 3D reconstruction of geological surfaces by
807 the equivalent dip-domain method: An example from field data of the Cerro Bayo
808 Anticline (Cordillera Oriental, NW Argentine Andes): Journal of Structural Geology,
809 v. 31, no. 12, p. 1573-1585.
810 Costa, E., Garcés, M., López-Blanco, M., Beamud, E., Gómez-Paccard, M., and Larrasoaña,
811 J. C., 2010, Closing and continentalization of the South Pyrenean foreland basin (NE
812 Spain): magnetochronological constraints: Basin Research, v. 22, no. 6, p. 904-917.
813 Cuenca, G., Canudo, J. I., Laplana, C., and Andrés, J. A., 1992, Bio y cronoestratigrafia con
814 mamíferos en la Cuenca Terciaria del Ebro: ensayo de síntesis: Acta Geológica
815 Hispánica, v. 27, no. 1-2, p. 127-143.
816 Cuevas, J. L., Arubués, P., Cabrera, L., and Marzo, M., 2007, Anatomy and architecture of
817 ephemeral, ribbon-like channel-fill deposits of the Caspe Formation (Upper Oligocene
818 to Lower Miocene of the Ebro Basin, Spain), *in* Nichols, G. J., Williams, E., and
819 Paola, C., eds., Sedimentary Processes, Environments and Basins: A Tribute to Peter
820 Friend: Oxford, Blackwell Publishing Ltd., p. 591-611.
821 Chen, Y., and Medioni, G., 1992, Object modelling by registration of multiple range images:
822 Image and Vision Computing, v. 10, no. 3, p. 145-155.

DeCelles, P. G., Gray, M. B., Ridgway, K. D., Cole, R. B., Pivnik, D. A., Pequera, N., and Srivastava, P., 1991, Controls on synorogenic alluvial-fan architecture, Beartooth Conglomerate (Palaeocene), Wyoming and Montana: Sedimentology, v. 38, no. 4, p. 567-590.

Donselaar, M. E., and Schmidt, J. M., 2005, Integration of outcrop and borehole image logs for high-resolution facies interpretation: example from a fluvial fan in the Ebro Basin, Spain: Sedimentology, v. 52, no. 5, p. 1021-1042.

Enge, H. D., Buckley, S. J., Rotevatn, A., and Howell, J. A., 2007, From outcrop to reservoir simulation model: Workflow and procedures: Geosphere, v. 3, no. 6, p. 469-490.

Faubel-Pérez, I., Hodgetts, D., and Redfern, J., 2009, A new approach for outcrop characterization and geostatistical analysis of a low-sinuosity fluvial-dominated succession using digital outcrop models: Upper Triassic Oukaimeden Sandstone Formation, central High Atlas, Morocco: AAPG Bulletin, v. 93, no. 6, p. 795-827.

-, 2010, Integration of digital outcrop models (DOMs) and high resolution sedimentology - workflow and implications for geological modelling: Oukaimeden Sandstone Formation, High Atlas (Morocco): Petroleum Geoscience, v. 16, no. 2, p. 133-154.

Fernández, O., 2005, Obtaining a best fitting plane through 3D georeferenced data: Journal of Structural Geology, v. 27, no. 5, p. 855-858.

Fernández, O., Muñoz, J. A., Arbués, P., Falivene, O., and Marzo, M., 2004, Three-dimensional reconstruction of geological surfaces: An example of growth strata and turbidite systems from the Ainsa basin (Pyrenees, Spain): AAPG Bulletin, v. 88, no. 8, p. 1049-1068.

Fisher, J. A., and Nichols, G. J., 2013, Interpreting the stratigraphic architecture of fluvial systems in internally drained basins: Journal of the Geological Society, v. 170, no. 1, p. 57-65.

Friend, P. F., Hirst, J. P. P., Hogan, P. J., Jolley, E. J., McElroy, R., Nichols, G. J., and Rodríguez, J., 1989, Pyrenean tectonic control of Oligo-Miocene river systems, Huesca, Aragón, Spain, *in* Marzo, M., and Puigdefàbregas, C., eds., 4th International Conference on Fluvial Sedimentology, Excursion guidebook nº4: Barcelona, Servei Geològic de Catalunya, p. 142.

Friend, P. F., Hirst, J. P. P., and Nichols, G. J., 1986, Sandstone-body structure and river process in the Ebro Basin of Aragón, Spain: Cuadernos de Geología Ibérica, v. 10, p. 9-30.

García-Sellés, D., Falivene, O., Arbués, P., Gratacós, O., Tavani, S., and Muñoz, J. A., 2011, Supervised identification and reconstruction of near-planar geological surfaces from terrestrial laser scanning: Computers & Geosciences, v. 37, p. 1584–1594.

Hajek, E. A., and Heller, P. L., 2012, Flow-Depth Scaling In Alluvial Architecture and Nonmarine Sequence Stratigraphy: Example from the Castlegate Sandstone, Central Utah, U.S.A: Journal of Sedimentary Research, v. 82, no. 2, p. 121-130.

Hamer, J. M. M., Sheldon, N. D., and Nichols, G. J., 2007a, Global Aridity during the Early Miocene? A Terrestrial Paleoclimate Record from the Ebro Basin, Spain: The Journal of Geology, v. 115, p. 601–608.

Hamer, J. M. M., Sheldon, N. D., Nichols, G. J., and Collinson, M. E., 2007b, Late Oligocene–Early Miocene paleosols of distal fluvial systems, Ebro Basin, Spain: Palaeogeography, Palaeoclimatology, Palaeoecology, v. 247, no. 3-4, p. 220-235.

Hartley, A. J., Weissmann, G. S., Nichols, G. J., and Warwick, G. L., 2010, Large Distributive Fluvial Systems: Characteristics, Distribution, and Controls on Development: Journal of Sedimentary Research, v. 80, no. 2, p. 167-183.

Hirst, J. P. P., 1991, Variations in alluvial architecture across the Oligo-Miocene Huesca Fluvial System, Ebro Basin, Spain, *in* Miall, A. D., and Tyler, N., eds., The three-

873 dimensional facies architecture of terrigenous clastic sediments and its implications
874 for hydrocarbon discovery and recovery: Tulsa, SEPM, p. 111-121.
875 Hirst, J. P. P., and Nichols, G. J., 1986, Thrust tectonic controls on Miocene alluvial
876 distribution patterns, southern Pyrenees, *in* Allen, P. A., and Homewood, P., eds.,
877 Foreland Basins, Volume 8: Oxford, Blackwell Scientific Publications, p. 247-258.
878 Janson, X., Kerans, C., Bellian, J. A., and Fitchen, W., 2007, Three-dimensional geological
879 and synthetic seismic model of Early Permian redeposited basinal carbonate deposits,
880 Victorio Canyon, west Texas: AAPG Bulletin, v. 91, no. 10, p. 1405-1436.
881 Jones, R. R., Kokklas, S., and McCaffrey, K. J. W., 2009, Quantitative analysis and
882 visualization of nonplanar fault surfaces using terrestrial laser scanning (LIDAR)—
883 The Arkitsa fault, central Greece, as a case study.: Geosphere, v. 5, no. 6, p. 465-482.
884 Jones, R. R., McCaffrey, K. J. W., Imber, J., Wightman, R., Smith, S. A., Holdsworth, R. E.,
885 Clegg, P., De Paola, N., Healy, D., and Wilson, R. W., 2008, Calibration and
886 validation of reservoir models: the importance of high resolution, quantitative outcrop
887 analogues, *in* Robinson, A., Griffiths, P., Price, S., Hegre, J., and Muggeride, A., eds.,
888 The Future of Geological Modelling in Hydrocarbon Development, The Geological
889 Society of London, p. 87-98.
890 Jones, R. R., Pringle, J. K., McCaffrey, K. J. W., Imber, J., Wightman, R., Guo, J., and Long,
891 J. J., 2011, Extending Digital Outcrop Geology into the Subsurface, *in* Martinsen, O.
892 J., Pulham, A. J., Haughton, P. D. W., and Sullivan, M. D., eds., Outcrops
893 Revitalized: Tools, Techniques and Applications, Volume 10, SEPM, p. 31-50.
894 Jones, S. J., 2004, Tectonic controls on drainage evolution and development of terminal
895 alluvial fans, southern Pyrenees, Spain: Terra Nova, v. 16, no. 3, p. 121-127.
896 Jones, S. J., Frostick, L. E., and Astin, T. R., 2001, Braided stream and flood plain
897 architecture: the Rio Vero Formation, Spanish Pyrenees: Sedimentary Geology, v.
898 139, no. 3-4, p. 229-260.
899 Jupp, P. E., Spurr, B. D., Nichols, G. J., and Hirst, J. P. P., 1987, Statistical estimation of the
900 apex of a sediment distribution system from paleocurrent data: Mathematical
901 Geology, v. 19, no. 4, p. 319-333.
902 Klise, K. A., Weissmann, G. S., McKenna, S. A., Nichols, E. M., Frechette, J. D.,
903 Wawrzyniec, T. F., and Tidwell, V. C., 2009, Exploring solute transport and
904 streamline connectivity using lidar-based outcrop images and geostatistical
905 representations of heterogeneity: Water Resources Research, v. 45, no. 5, p. W05413.
906 Kreylos, O., Oskin, M., Cowgill, E., Gold, P., Elliott, A., and Kellogg, L. H., 2013, Point-
907 based computing on scanned terrain with LidarViewer: Geosphere, v. 9, no. 3, p. 546-
908 556.
909 Labourdette, R., 2011, Stratigraphy and static connectivity of braided fluvial deposits of the
910 lower Escanilla Formation, south central Pyrenees, Spain: AAPG Bulletin, v. 95, no.
911 4, p. 585.
912 Labourdette, R., and Jones, R. R., 2007, Characterization of fluvial architectural elements
913 using a three-dimensional outcrop data set: Escanilla braided system, South-Central
914 Pyrenees, Spain: Geosphere, v. 3, no. 6, p. 422-434.
915 Li, W., Bhattacharya, J. P., and Zhu, Y., 2012, Stratigraphic uncertainty in sparse versus rich
916 data sets in a fluvial-deltaic outcrop analog: Ferron Notom delta in the Henry
917 Mountains region, southern Utah: AAPG Bulletin, v. 96, no. 3, p. 415-438.
918 Lichti, D. D., 2004, A resolution measure for terrestrial laser scanners, *in* Altan, O., ed., XXth
919 ISPRS Congress, Volume 34: Istambul, Turkay, The International Archives of the
920 Photogrammetry, Remote Sensing and Spatial Information Sciences, p. 216-221.

921 Luzón, A., 2005, Oligocene–Miocene alluvial sedimentation in the northern Ebro Basin, NE
922 Spain: Tectonic control and palaeogeographical evolution Sedimentary Geology, v.
923 177, no. 1-2, p. 19-39.
924 Luzón, A., and González, A., 2003, Los sistemas aluviales oligo-miocenos del margen N de
925 la Cuenca del Ebro: Caracterización sedimentaria y síntesis paleogeográfica: Revista
926 de la Sociedad Geológica de España, v. 16, no. 3-4, p. 239-255.
927 Martinius, A. W., and Næss, A., 2005, Uncertainty analysis of fluvial outcrop data for
928 stochastic reservoir modelling: Petroleum Geoscience, v. 11, no. 3, p. 203-214.
929 McCaffrey, K. J. W., Jones, R. R., Holdsworth, R. E., Wilson, R. W., Clegg, P., Imber, J.,
930 Holliman, N. S., and Trinks, I., 2005, Unlocking the spatial dimension : digital
931 technologies and the future of geoscience fieldwork: Journal of the Geological
932 Society, v. 162, no. 2, p. 927-938.
933 Miall, A. D., 1988, Facies architecture in clastic sedimentary basins, New perspectives in
934 basin analysis, Springer, p. 67-81.
935 -, 1996, The Geology of Fluvial Deposits: Sedimentary Facies, Basin Analysis, and
936 Petroleum Geology, Heidelberg, Springer-Verlag Inc., 582 p.
937 -, 2006, Reconstructing the architecture and sequence stratigraphy of the preserved fluvial
938 record as a tool for reservoir development: A reality check: AAPG Bulletin, v. 90, no.
939 7, p. 989-1002.
940 Möhrig, D., Heller, P. L., Paola, C., and Lyons, W. J., 2000, Interpreting avulsion process
941 from ancient alluvial sequences: Guadalope-Matarranya system (northern Spain) and
942 Wasatch Formation (western Colorado): GSA Bulletin, v. 112, no. 12, p. 1787-1803.
943 Nichols, E. M., Weissmann, G. S., Wawrzyniec, T. F., Frechette, J. D., and Klise, K. A.,
944 2011, Processing of outcrop-based LIDAR imagery to characterize heterogeneity for
945 groundwater models, *in* Martinsen, O. J., Pulham, A. J., Haughton, P. D. W., and
946 Sullivan, M. D., eds., Outcrops Revitalized: Tools, Techniques and Applications,
947 SEPM, p. 239–247.
948 Nichols, G. J., 2004, Sedimentation and base level in an endorheic basin: the early Miocene
949 of the Ebro Basin, Spain: Boletín Geológico y Minero, v. 115, no. 3, p. 427-438.
950 -, 2005, Tertiary alluvial fans at the northern margin of the Ebro Basin: a review, *in* Harvey,
951 A. M., Mather, A. E., and Stokes, M., eds., Alluvial Fans: Geomorphology,
952 Sedimentology, Dynamics.: London, The Geological Society of London, p. 187-206.
953 -, 2007, Fluvial systems in desiccating endorheic basins, *in* Nichols, G. J., Williams, E., and
954 Paola, C., eds., Sedimentary Processes, Environments and Basins: A Tribute to Peter
955 Friend, International Association of Sedimentologists.
956 -, 2012, Endorheic Basins, *in* Busby, C., and Azor, A., eds., Tectonics of Sedimentary Basins:
957 Recent advances, Wiley-Blackwell, p. 621-632.
958 Nichols, G. J., and Fisher, J. A., 2007, Processes, facies and architecture of fluvial
959 distributary system deposits: Sedimentary Geology, v. 195, no. 1-2, p. 75-90.
960 Nichols, G. J., and Hirst, J. P. P., 1998, Alluvial fans and fluvial distributary systems, Oligo-
961 Miocene, northern Spain: contrasting processes and products: Journal of Sedimentary
962 Research, v. 68, no. 5, p. 879-889.
963 North, C. P., and Prosser, D. J., 1993, Characterization of fluvial and aeolian reservoirs:
964 problems and approaches, *in* North, C. P., and Prosser, D. J., eds., Characterization of
965 Fluvial and Aeolian Reservoirs, Volume 73: London, The Geological Society of
966 London, p. 1-6.
967 Odin, G. S., Cuenca, G., Canudo, J. I., Cosca, M., and Lago, M., 1997, Biostratigraphy and
968 Geochronology of a Miocene continental volcaniclastic layer from the Ebro Basin,
969 Spain, *in* Montanari, A., Odin, G. S., and Coccioni, R., eds., Miocene Stratigraphy:
970 An Integrated Approach: Amsterdam, Elsevier, p. 297-310.

971 Olariu, M. I., Aiken, C. L. V., Bhattacharya, J. P., and Xu, X., 2011, Interpretation of
972 channelized architecture using three-dimensional photo real models, Pennsylvanian
973 deep-water deposits at Big Rock Quarry, Arkansas: Marine and Petroleum Geology,
974 v. 28, no. 6, p. 1157-1170.
975 Olariu, M. I., Ferguson, J. F., Aiken, C., and Xu, X., 2008, Outcrop fracture characterization
976 using terrestrial laser scanners: Deep-water Jackfork sandstone at Big Rock Quarry,
977 Arkansas: Geosphere, v. 4, no. 1, p. 247-259.
978 Olariu, M. I., Olariu, C., Steel, R. J., Dalrymple, R. W., and Martinius, A. W., 2012,
979 Anatomy of a laterally migrating tidal bar in front of a delta system: Esdolomada
980 Member, Roda Formation, Tremp-Graus Basin, Spain: Sedimentology, v. 59, no. 2, p.
981 356-378.
982 Pearce, M. A., Jones, R. R., Smith, S. A., and McCaffrey, K. J. W., 2011, Quantification of
983 fold curvature and fracturing using terrestrial laser scanning: AAPG Bulletin, v. 95,
984 no. 5, p. 771-794.
985 Phelps, R. M., and Kerans, C., 2007, Architectural Characterization and Three-Dimensional
986 Modeling of a Carbonate Channel–Levee Complex: Permian San Andres Formation,
987 Last Chance Canyon, New Mexico, U.S.A: Journal of Sedimentary Research, v. 77,
988 no. 11, p. 939-964.
989 Pranter, M. J., Cole, R. D., Panjaitan, H., and Sommer, N. K., 2009, Sandstone-body
990 dimensions in a lower coastal-plain depositional setting: Lower Williams Fork
991 Formation, Coal Canyon, Piceance Basin, Colorado: AAPG Bulletin, v. 93, no. 10, p.
992 1379-1401.
993 Pranter, M. J., Ellison, A. I., Cole, R. D., and Patterson, P. E., 2007, Analysis and modeling
994 of intermediate-scale reservoir heterogeneity based on a fluvial point-bar outcrop
995 analog, Williams Fork Formation, Piceance Basin, Colorado: AAPG Bulletin, v. 91,
996 no. 7, p. 1025-1051.
997 Pringle, J. K., Brunt, R. L., Hodgson, D. M., and Flint, S. S., 2010, Capturing stratigraphic
998 and sedimentological complexity from submarine channel complex outcrops to digital
999 3D models, Karoo Basin, South Africa: Petroleum Geoscience, v. 16, no. 4, p. 307-
1000 330.
1001 Pringle, J. K., Gardiner, A., and Westerman, R., 2004, Topics: Virtual geological outcrops –
1002 fieldwork and analysis made less exhaustive?: Geology Today, v. 20, no. 2, p. 67-71.
1003 Pringle, J. K., Howell, J. A., Hodgetts, D., Westerman, A. R., and Hodgson, D. M., 2006,
1004 Virtual outcrop models of petroleum reservoir analogues: a review of the current
1005 state-of-the-art: First Break, v. 24, p. 33-42.
1006 Puigdefàbregas, C., Muñoz, J. A., and Vergès, J., 1992, Thrusting and foreland basin
1007 evolution in the Southern Pyrenees, *in* McClay, K. R., ed., Thrust Tectonics: London,
1008 Chapman & Hall, p. 247-254.
1009 Puigdefábregas, C., Nijman, W., and Muñoz, J. A., 1991, Alluvial deposits of the successive
1010 foreland basin stages and their relation to the Pyrenean thrust sequences, Barcelona,
1011 Servei Geològic de Catalunya, Guidebook Series of the 4th International Conference
1012 on Fluvial Sedimentology, 176 p.
1013 Puigdefàbregas, C., and Souquet, P., 1986, Tecto-sedimentary cycles and depositional
1014 sequences of the Mesozoic and Tertiary from the Pyrenees: Tectonophysics, v. 129,
1015 no. 1-4, p. 173-203.
1016 Pyles, D. R., Jennette, D. C., Tomasso, M., Beaubouef, R. T., and Rossen, C., 2010, Concepts
1017 Learned from a 3D Outcrop of a Sinuous Slope Channel Complex: Beacon Channel
1018 Complex, Brushy Canyon Formation, West Texas, U.S.A: Journal of Sedimentary
1019 Research, v. 80, no. 1, p. 67-96.

Quirantes, J., 1969, Estudio sedimentológico y estratigráfico del Terciario continental de los Monegros. [Ph.D. thesis]: Zaragoza, Universidad de Zaragoza, 105 p.
Ring, J., 1963, The laser in astronomy: New Scientist, v. 18, no. 344, p. 672-673.
Rittersbacher, A., Howell, J. A., and Buckley, S. J., 2014, Analysis Of Fluvial Architecture In the Blackhawk Formation, Wasatch Plateau, Utah, U.S.A., Using Large 3D Photorealistic Models: Journal of Sedimentary Research, v. 84, no. 2, p. 72-87.
Sahoo, H., and Gani, N. D., 2015, Creating three-dimensional channel bodies in LiDAR-integrated outcrop characterization: A new approach for improved stratigraphic analysis: Geosphere, v. 11, no. 3, p. 777-785.
Tomasso, M., Bouroullec, R., and Pyles, D. R., 2010, The use of spectral recomposition in tailored forward seismic modeling of outcrop analogs: AAPG Bulletin, v. 94, no. 4, p. 457-474.
van Lanen, X. M. T., Hodgetts, D., Redfern, J., and Faubel-Pérez, I., 2009, Applications of digital outcrop models: two fluvial case studies from the Triassic Wolfville Fm., Canada and Oukaimeden Sandstone Fm., Morocco: Geological Journal, v. 44, no. 6, p. 742-760.
Ventra, D., Nichols, G. J., and Mountney, N., 2014, Autogenic dynamics of alluvial fans in endorheic basins: Outcrop examples and stratigraphic significance: Sedimentology, v. 61, no. 3, p. 767-791.
Verwer, K., Merino-Tomé, O., Kenter, J. A. M., and Della Porta, G., 2009, Evolution of a High-Relief Carbonate Platform Slope Using 3D Digital Outcrop Models: Lower Jurassic Djebel Bou Dahar, High Atlas, Morocco: Journal of Sedimentary Research, v. 79, no. 6, p. 416-439.
Vincent, S. J., 2001, The Sis palaeovalley: a record of proximal fluvial sedimentation and drainage basin development in response to Pyrenean mountain building: Sedimentology, v. 48, no. 6, p. 1235-1276.
Vincent, S. J., and Elliott, T., 1997, Long-lived Transfer-Zone Paleovalleys in Mountain Belts: An Example from the Tertiary of the Spanish Pyrenees: Journal of Sedimentary Research, v. 67, no. 2, p. 303-310.
Webber, K. J., and van Geuns, L. C., 1990, Framework for Constructing Clastic Reservoir Simulation Models: Journal of Petroleum Technology, v. 42, no. 10, p. 1248-1297.
Wilson, C. E., Aydin, A., Karimi-Fard, M., Durlofsky, L. J., Sagy, A., Brodsky, E. E., Kreylos, O., and Kellogg, L. H., 2011, From outcrop to flow simulation: Constructing discrete fracture models from a LIDAR survey: AAPG Bulletin, v. 95, no. 11, p. 1883-1905.
Wilson, P., Hodgetts, D., Rarity, F., Gawthorpe, R. L., and Sharp, I. R., 2009, Structural geology and 4D evolution of a half-graben: New digital outcrop modelling techniques applied to the Nukhul half-graben, Suez rift, Egypt: Journal of Structural Geology, v. 31, no. 3, p. 328-345.
Willis, B. J., and White, C. D., 2000, Quantitative Outcrop Data for Flow Simulation: Journal of Sedimentary Research, v. 70, no. 4, p. 788-802.
Wise, D. U., 1992, Dip domain method applied to the Mesozoic Connecticut Valley Rift Basins: Tectonics, v. 11, no. 6, p. 1357-1368.
Woodcock, N. H., 1977, Specification of fabric shapes using an eigenvalue method: Geological Society of America Bulletin, v. 88, no. 9, p. 1231-1236.
Yuste, A., Luzón, A., and Bauluz, B., 2004, Provenance of Oligocene–Miocene alluvial and fluvial fans of the northern Ebro Basin (NE Spain): an XRD, petrographic and SEM study: Sedimentary Geology, v. 172, no. 3-4, p. 251-268.

## FIGURE CAPTIONS

Figure 1. Geological map of the North-Central Ebro Basin showing the location of the outcrops and the distribution of the Oligo-Miocene facies of the Huesca Fluvial Fan and the adjacent lacustrine system (modified from Nichols and Hirst, 1998). Location of the apex of the fluvial system was estimated by Jupp et al. (1987) based on a statistical analysis of the paleocurrents. Tectonic features: SPFT-South Pyrenean Frontal Thrust; BA-Barbasto Anticline. Cities: A-Ayerbe; B-Barbastro; F-Fraga; M-Monzón; S-Sariñena. Rivers: Al-Alcanadre; Ci-Cinca: Eb-Ebro; Fl-Flúmen; Gá-Gállego.

Figure 2. Topographical maps draped onto a shaded DEM of the Montearagón (A) and Piracés (B) outcrops. The extent of the scanned areas, the location of the scanning stations and the trajectories of the stratigraphic logs are indicated. Two panoramic views of the DOM, one with only an artificial lighting and the other with a color texture are provided for each of the numbered scanning stations (1 and 2 from Montearagón; 3 to 5 from Piracés).

Figure 3. Detail of the Montearagón DOM displayed with an orthogonal projection showing the trajectory of the stratigraphic log MA5. The log is presented on the right together with the depositional interpretation of several sandstone intervals. Application of the method explained in the section "Results and practical applications" sows how the heights and thicknesses of the sandstone bodies in the log match those observed in the DOM. Labeled boxes highlight the presence of a levee (A) and a channel "wing" (B).

Figure 4. Flow diagram depicting the series of steps and verifications that must be followed to obtain a suitable Virtual Datum.

Figure 5. Conceptual scheme of a sinuous (A) and straight (B) channel of the Huesca Fluvial Fan showing how the upper surface (red dashed line) of sandstone bodies (orange) can be used to infer the orientation of the depositional surface (green surface).

1094 Figure 6. Detail of the Piracés DOM displayed in an orthogonal projection (A, see location in
1095 Figure 2). The upper boundaries of sandstone bodies were digitized in two ways: strictly
1096 following their tops (B), and depicting flat upper envelopes (C). Differences arising from
1097 these two methods of digitizing (D) are related to the depositional topography (e.g., clay
1098 plugs and levees), post-depositional erosive events, outcropping conditions (1) and
1099 concealment of part of the outcrop due to perspective issues during acquisition (2). Note how
1100 some large internal scours within the paleochannels are laterally related to the top of other
1101 sandstone bodies (black arrows), suggesting that they are interrelated.
1102 Figure 7. Comparison between the DOM displayed with a perspective (A) or an orthogonal
1103 (B) projection. The two images show the same area of the Montearagón DOM (the SE
1104 boundary), and were captured from the same viewpoint. Colored lines represent the
1105 intersection with the DOM of several flat stratigraphic surfaces traced with a Virtual Datum.
1106 Using an orthogonal projection they are displayed as straight lines (B), whereas with a
1107 perspective projection this only occurs when the observer is at the same height as the surface
1108 (light blue line in A).
1109 Figure 8. Detail of the Montearagón DOM displayed with an orthogonal projection (see
1110 location in Figure 2) where the plane calculated from a polyline together with the method to
1111 verify its intersection with the DOM are shown. After selecting the nearest points to the
1112 polyline (A), the macro (see text) calculates the plane that best fits them and includes it in the
1113 scene. As a result, the data located behind the plane are concealed (B). This is solved by
1114 selecting those points that are located within a narrow range from it, which results in a line
1115 that allows us to remove the plane and verify its geometrical relationship with respect to the
1116 stratigraphy (C).
1117 Figure 9. Orthogonal views of the Montearagón DOM (A and B; see location in Figure 2)
1118 where two erroneous correlation planes that clearly intersect stratigraphic horizons are shown

(A' and B'). By using a Virtual Datum (A'' and B''), the interpreted stratigraphic horizons are parallel to the remaining ones and connect the paleochannels with sandstone bodies that were previously interpreted as unrelated (pink boxes).

Figure 10. Panoramic views using an orthogonal projection of three areas of the Montearagón DOM: Montearagón E (A), Montearagón W (B) and Barranco Hondo W (C; see their exact location in D). The lines result from using the Virtual Datum to outline several stratigraphic intervals, which are shown with the same color in all the images. Note how the upper boundaries of some sandstone bodies are not represented by a single stratigraphic surface (E, F), suggesting a multi-stage depositional history.

Figure 11. Oblique views showing the full extent of the Montearagón (A to E) and Piracés (F to H) DOMs. Red intervals represent stratigraphic intervals that were obtained by placing the Virtual Datum over a large paleochannel and by selecting all the points located below the datum to a distance equal to the maximum thickness of the paleochannel (9 m for Montearagón and 21 m for Piracés). Stratigraphic intervals can be isolated (B and G), which facilitates their subsequent study and reconstruction. C, D and E are details of the stratigraphic interval isolated in B; and H is a view towards the west of the stratigraphic interval shown in G.

Figure 12. Correlation panel composed of the seven stratigraphic logs measured in the Montearagón outcrop (see its location in Figure 2), which were previously corrected using the method described. Body-to-body correlations were performed with the Virtual Datum, and tilting of the series was restored to horizontal. The classification of sandstone levels was carried out according to the geometrical and architectural criteria established by Friend et al. (1986). There is no information about the zone below the Montearagón Castle because it was not captured during the acquisition campaign.

Figure 1
Click here to download Figure: Figure 1.png

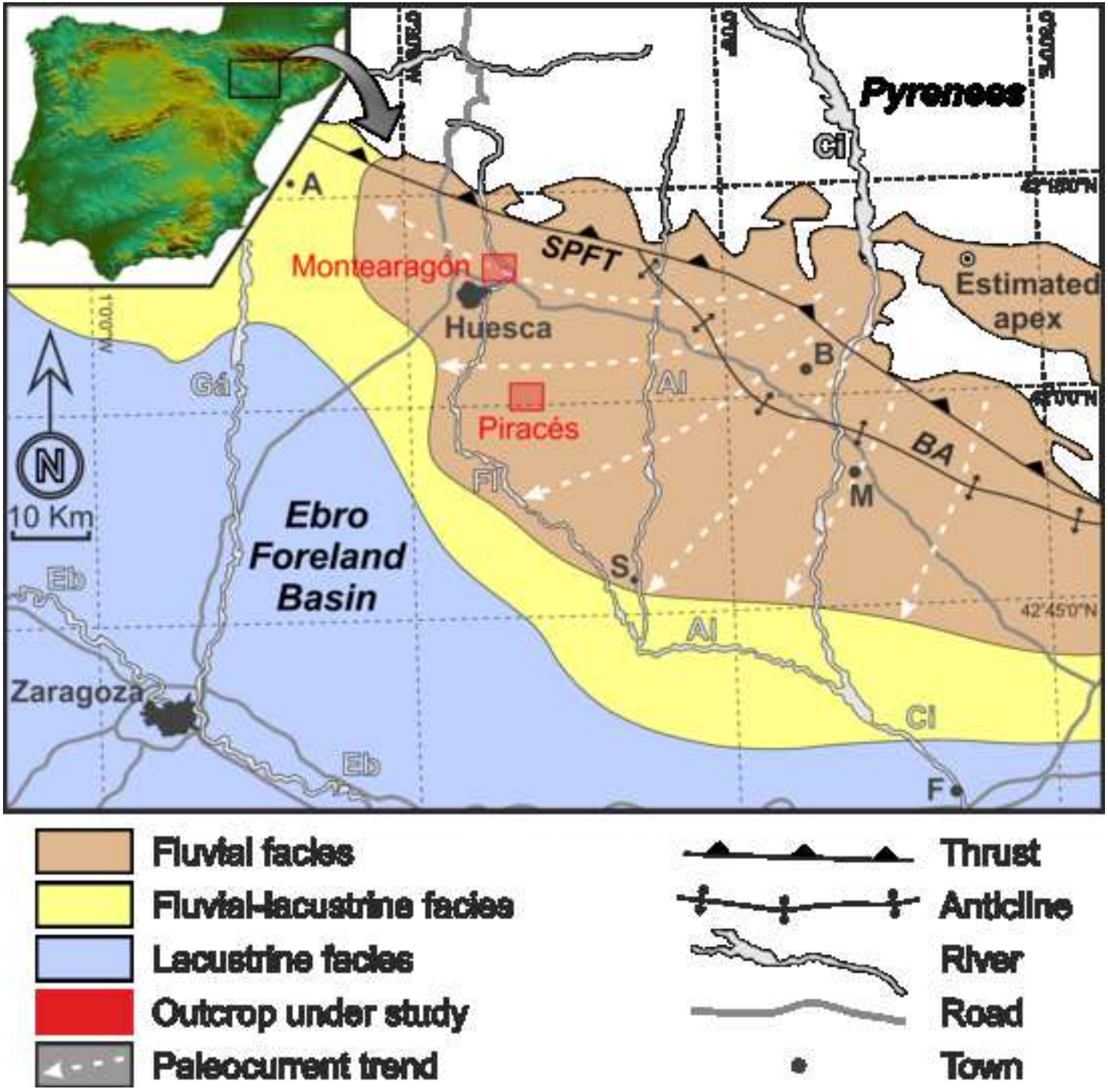

Figure 2
Click here to download Figure: Figure 2.png

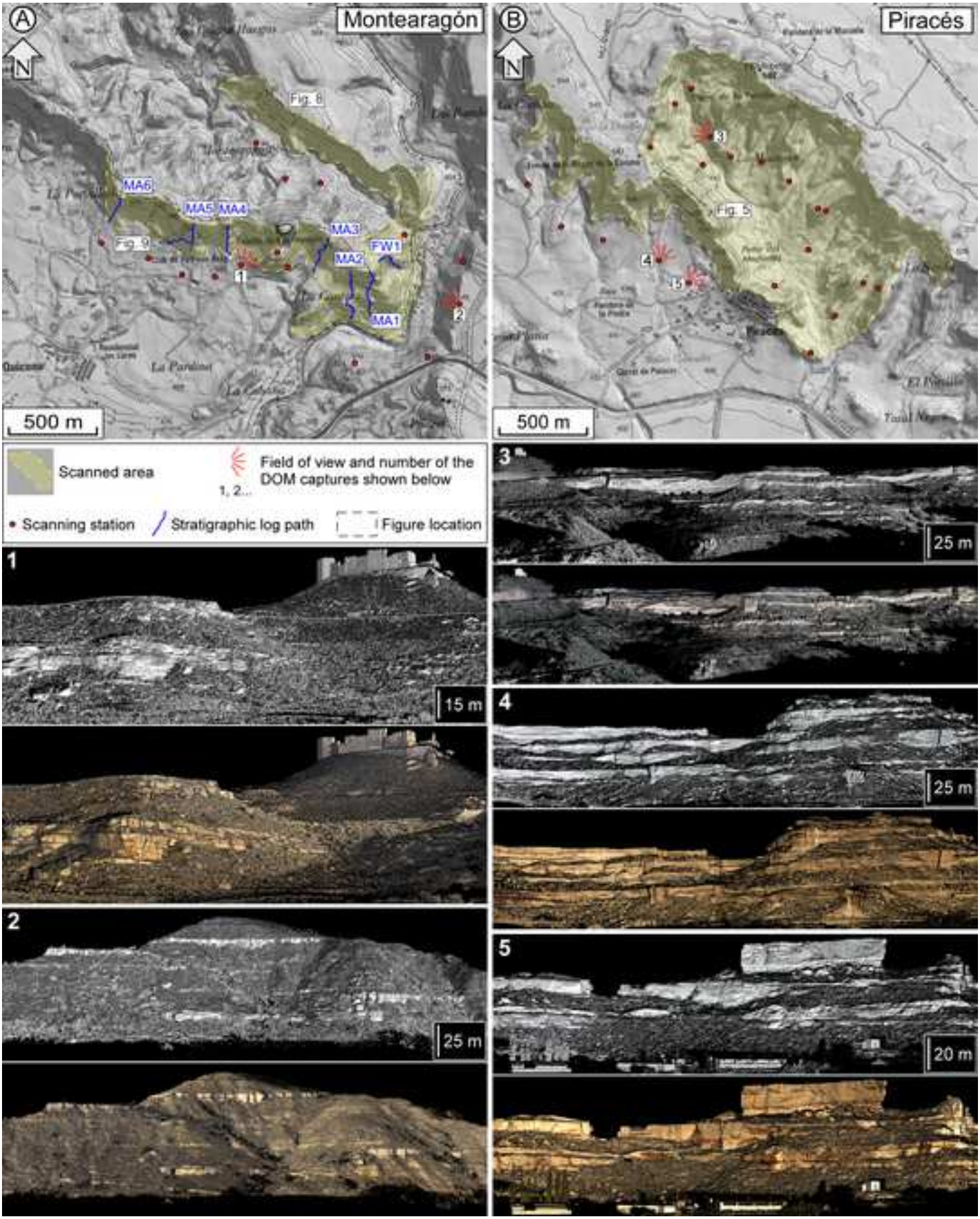

Figure 3
Click here to download Figure: Figure 3.png

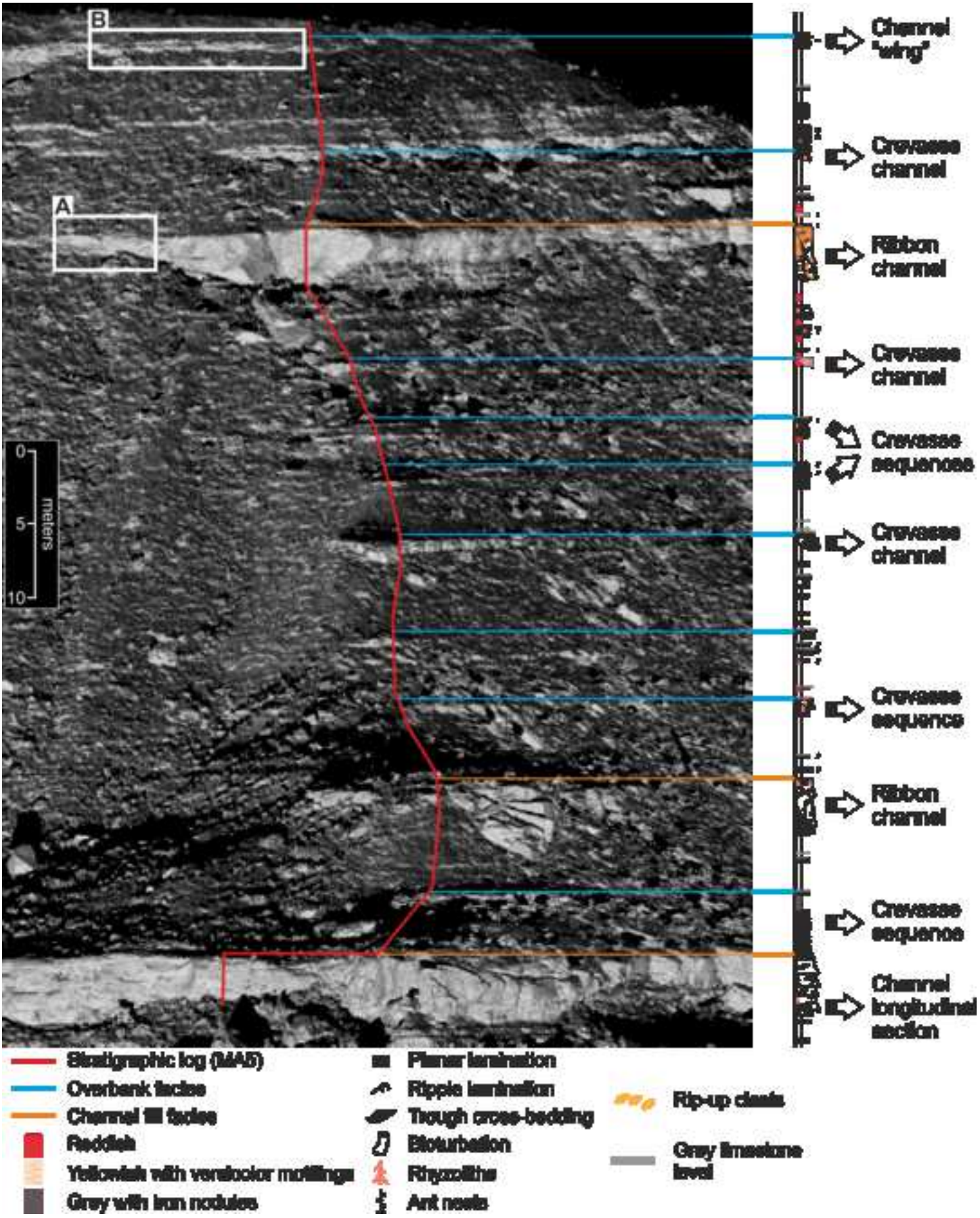

Figure 4
Click here to download Figure: Figure 4.png

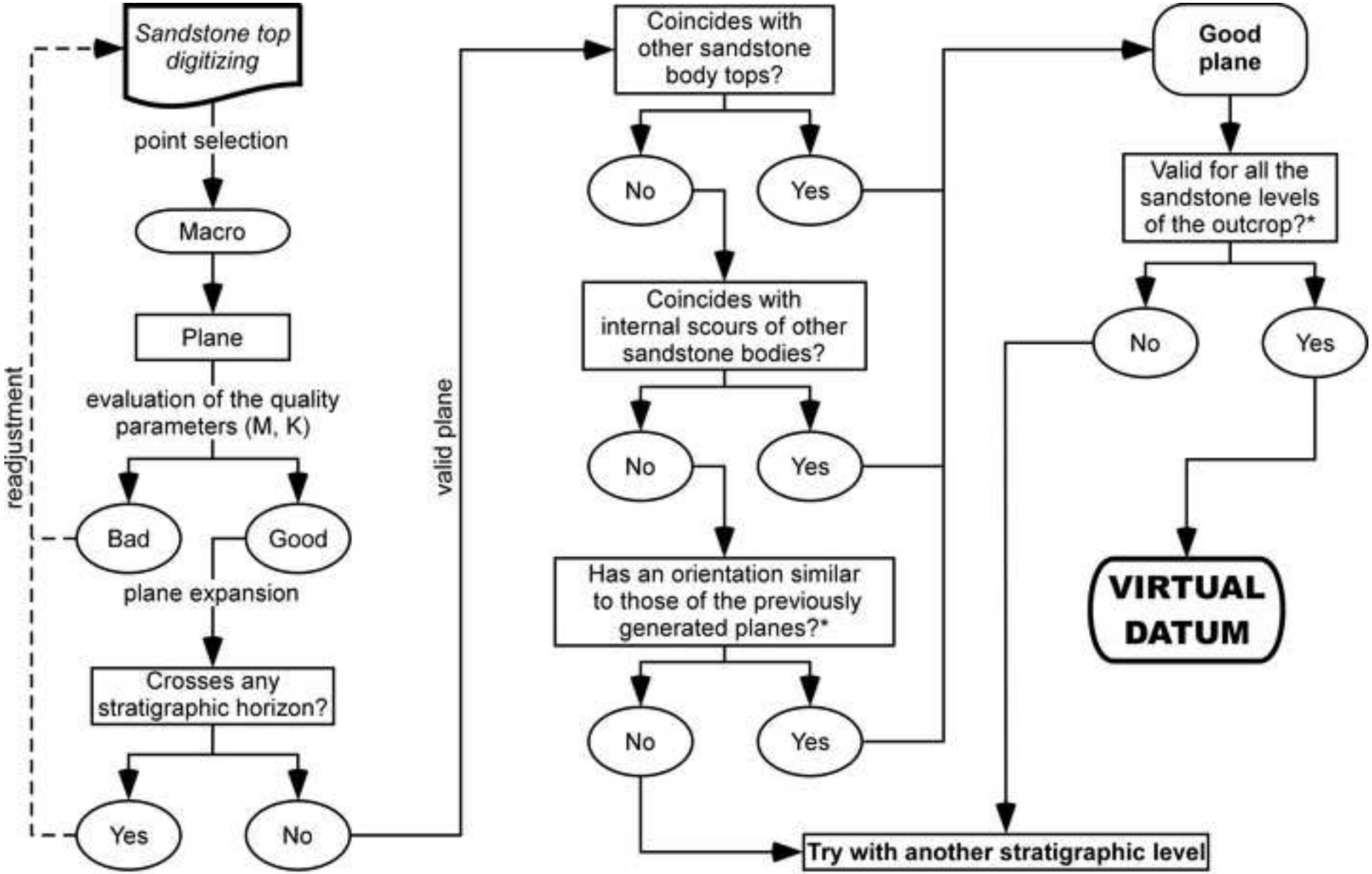


*Assuming that the outcrop lacks angular unconformities. Otherwise the question will refer only to the stratigraphic interval from which the plane was calculated.

Figure 5
Click here to download Figure: Figure 5.png

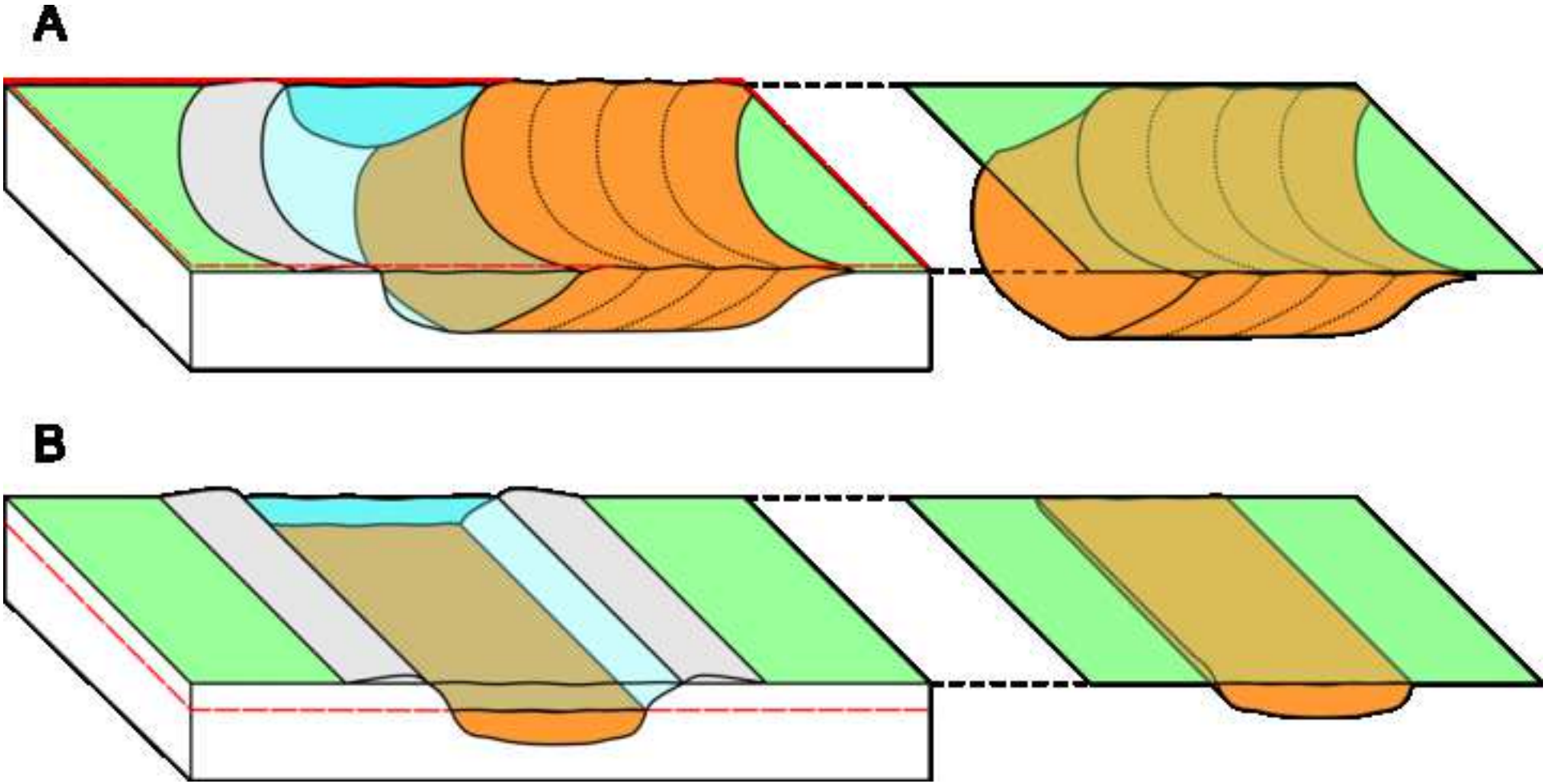

Figure 6
Click here to download Figure: Figure 6.jpg

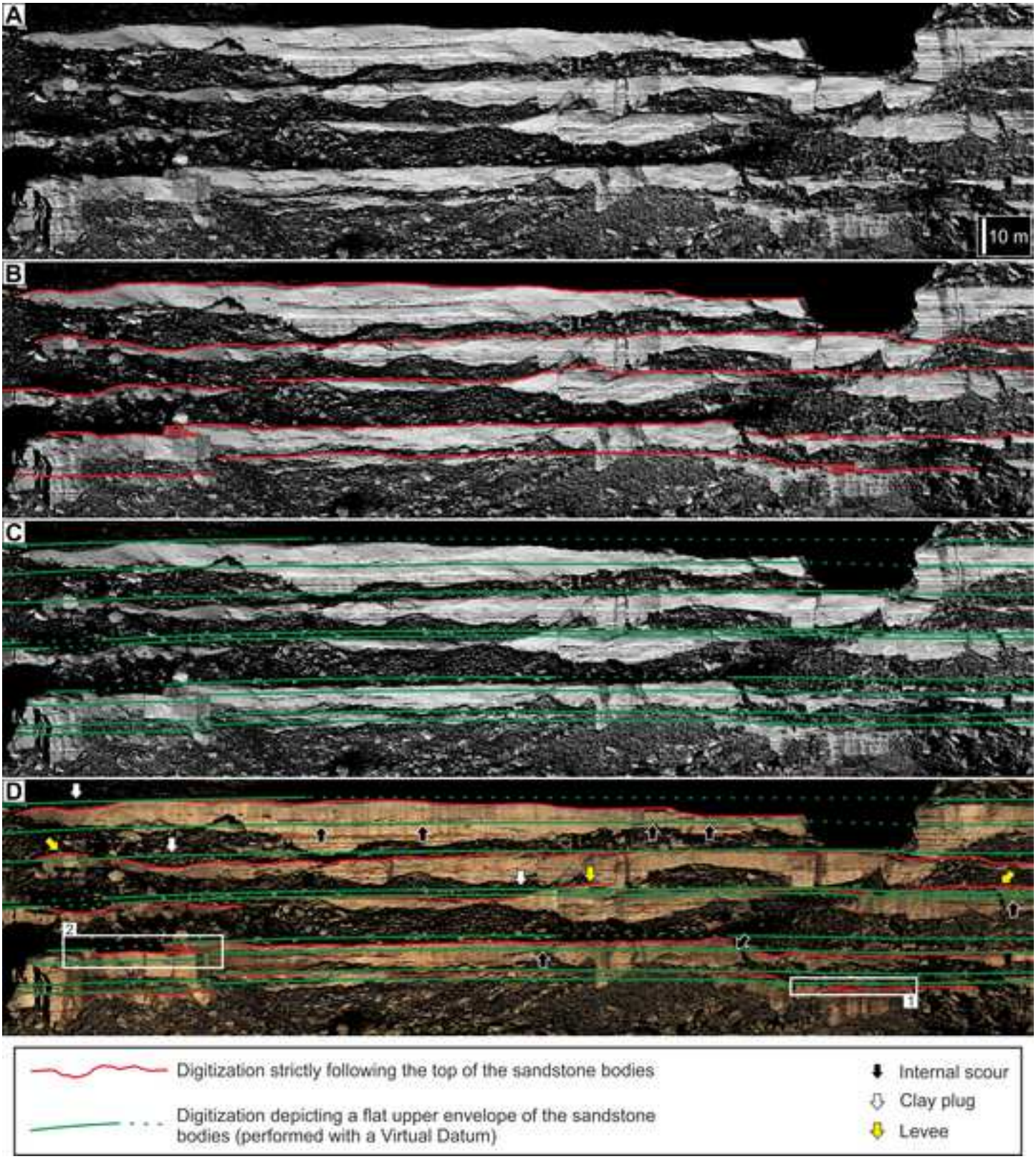

Figure 7
Click here to download Figure: Figure 7.png

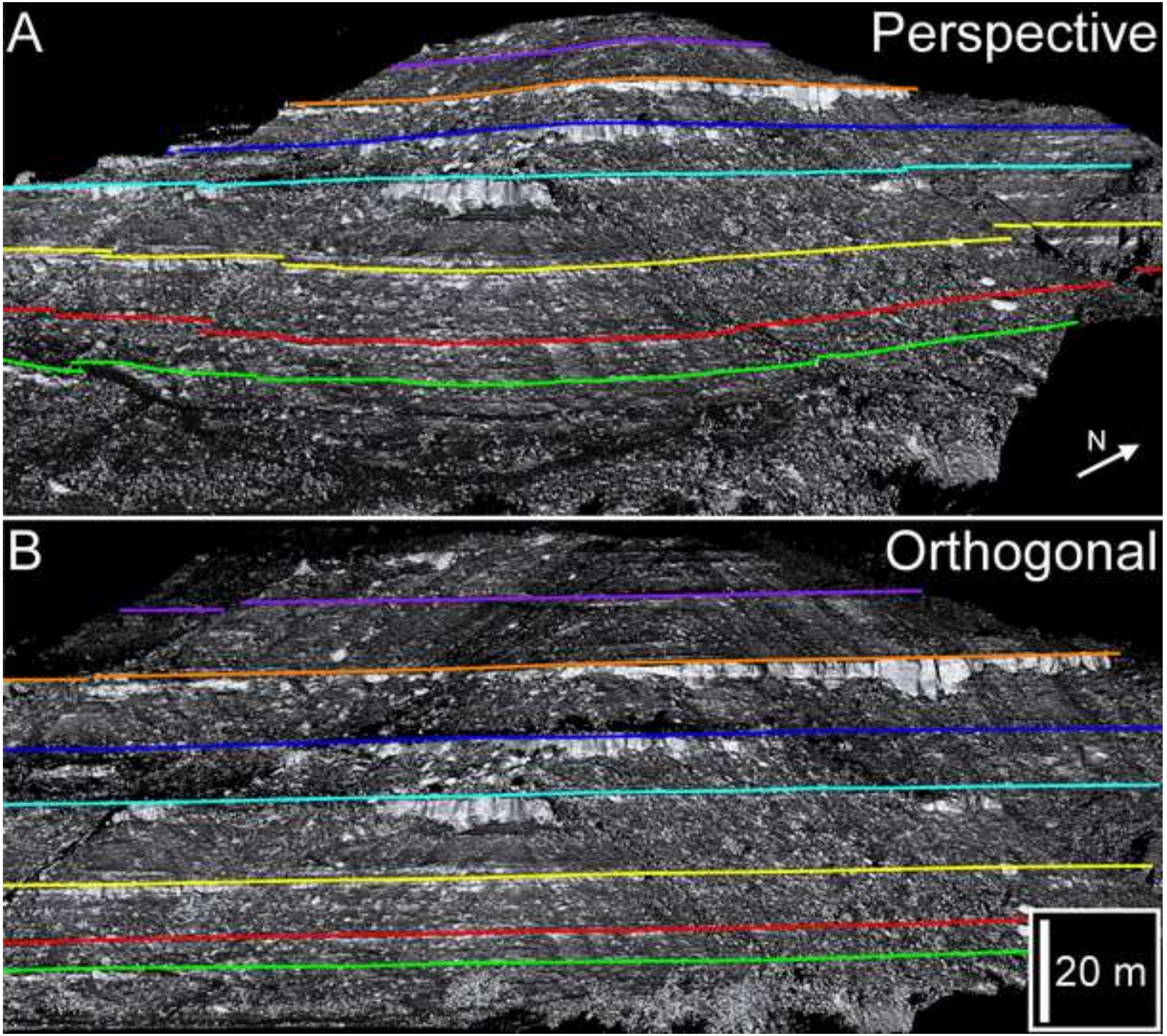

Figure 8
Click here to download Figure: Figure 8.png

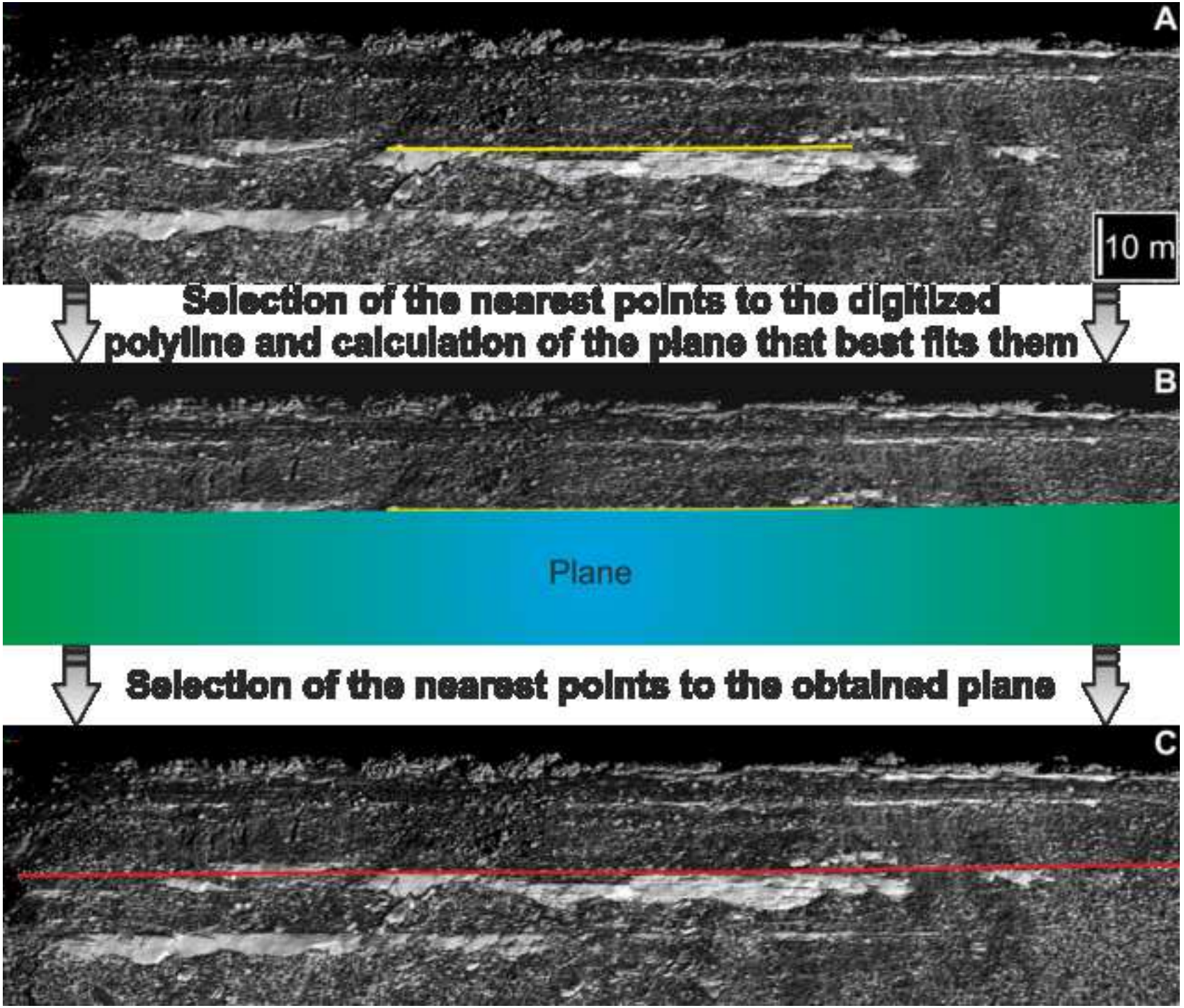

Figure 9

Click here to download Figure: Figure 9.png

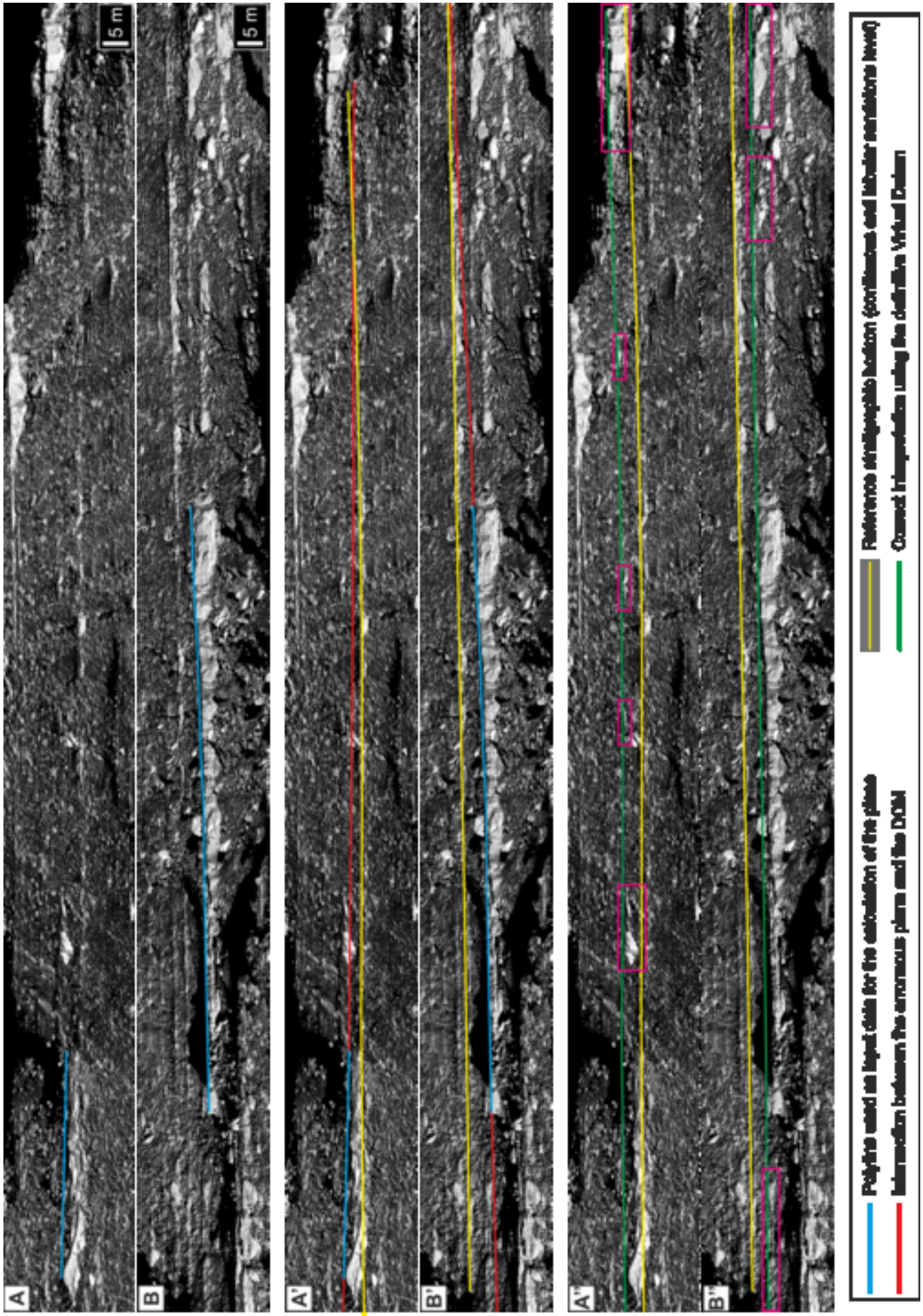

Figure 10
Click here to download Figure: Figure 10.png

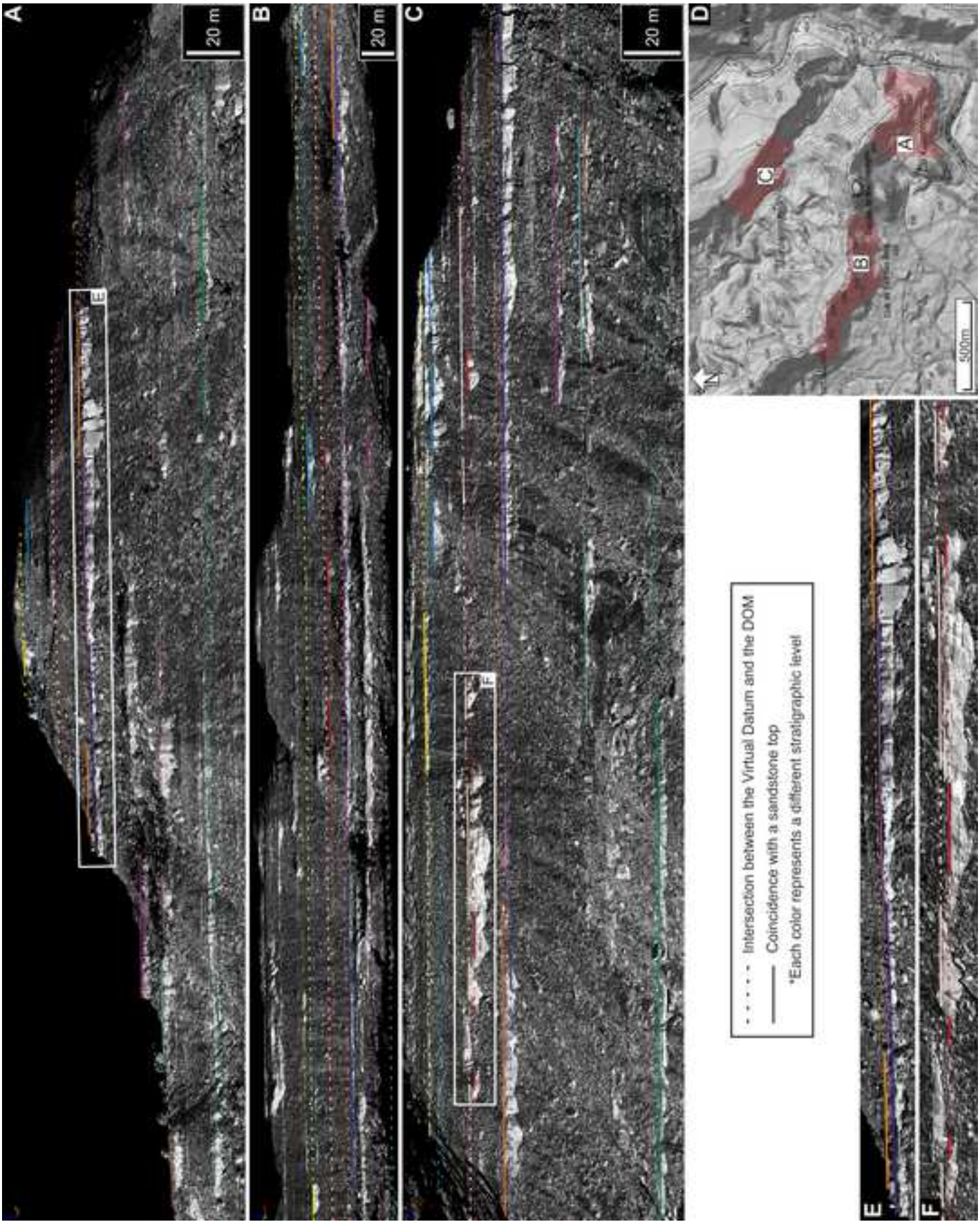

Figure 11_1
Click here to download Figure: Figure 11_1.png

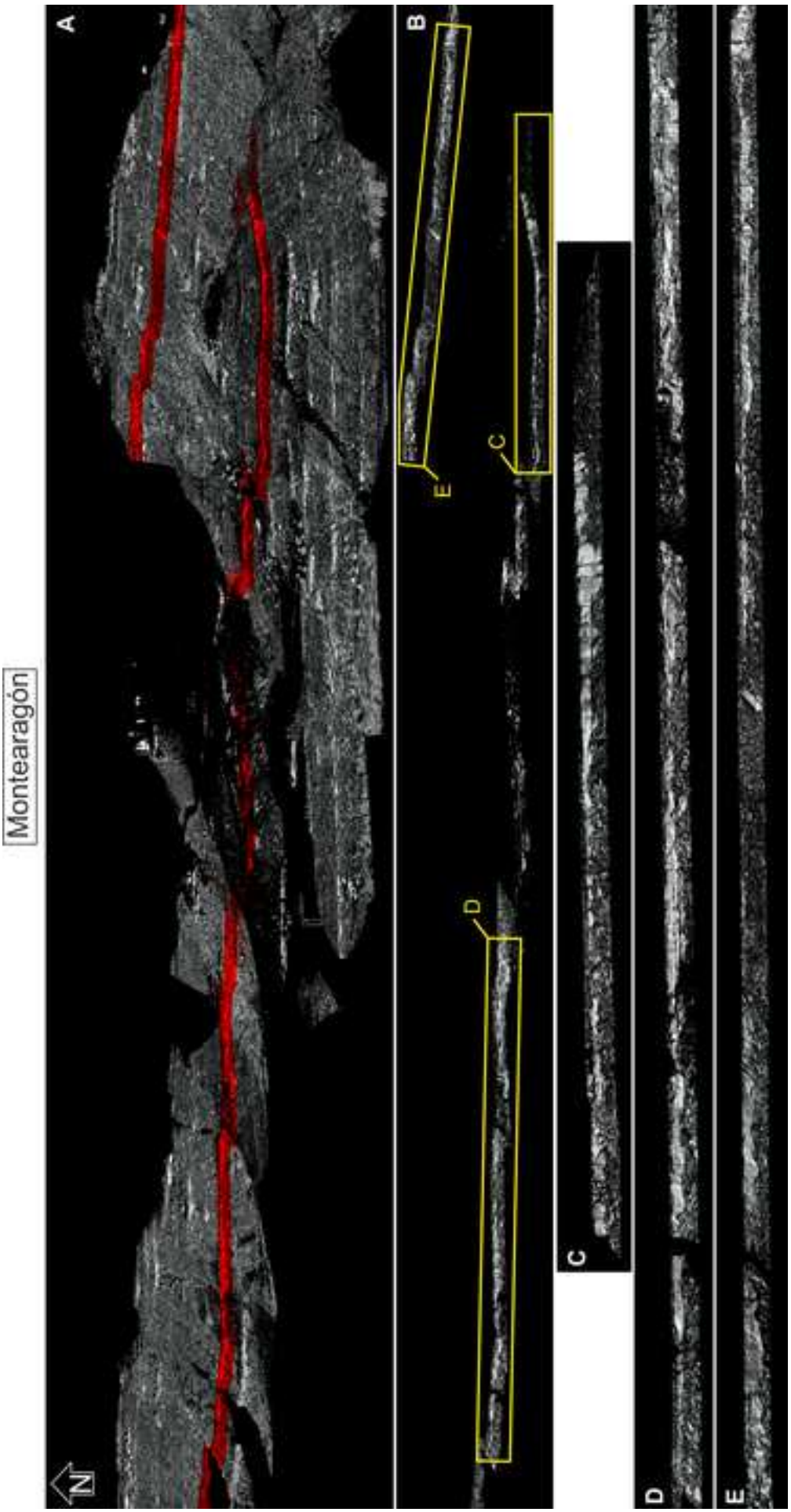

Figure 11_2
Click here to download Figure: Figure 11_2.png

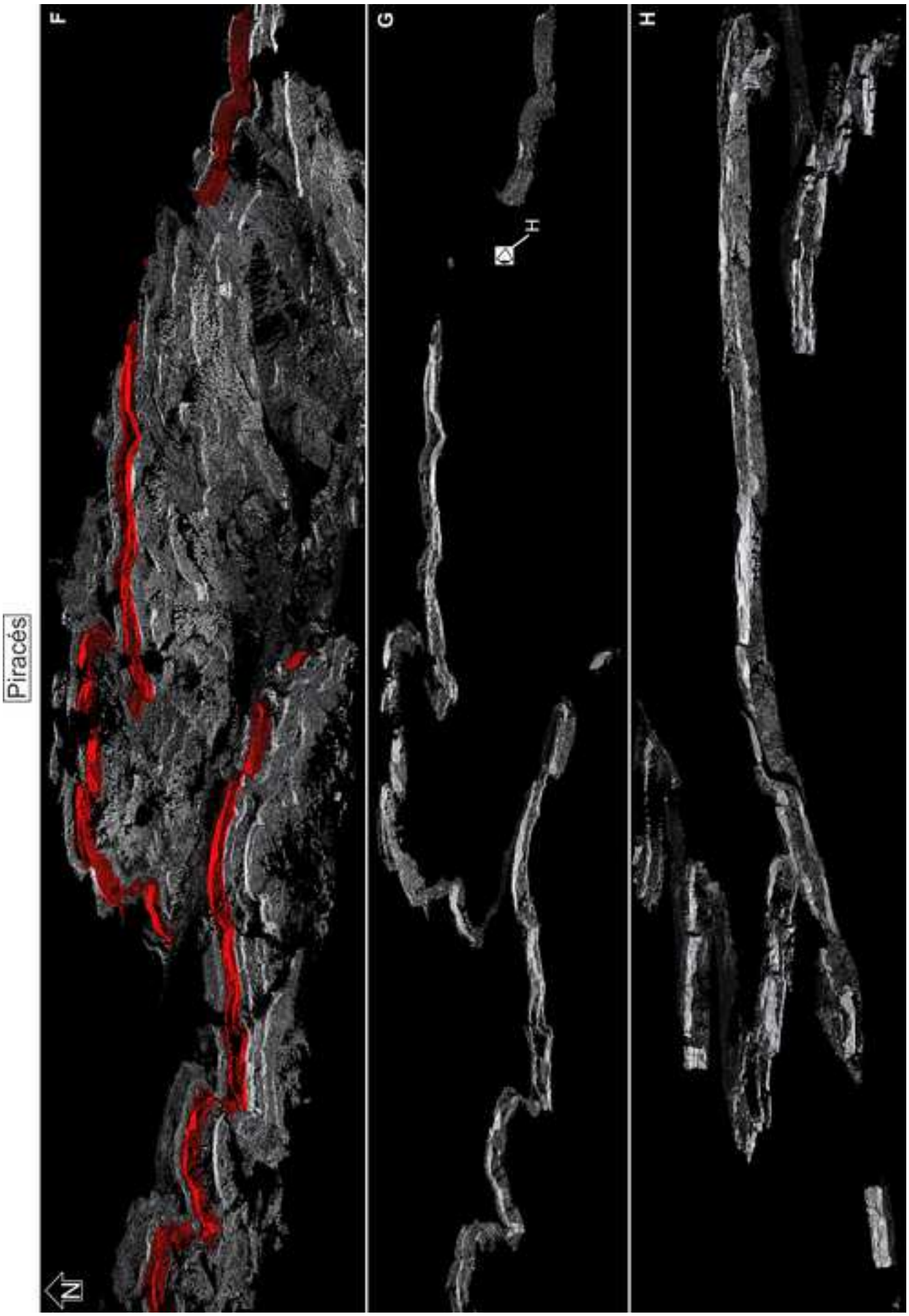

Figure 12
Click here to download Figure: Figure 12.png

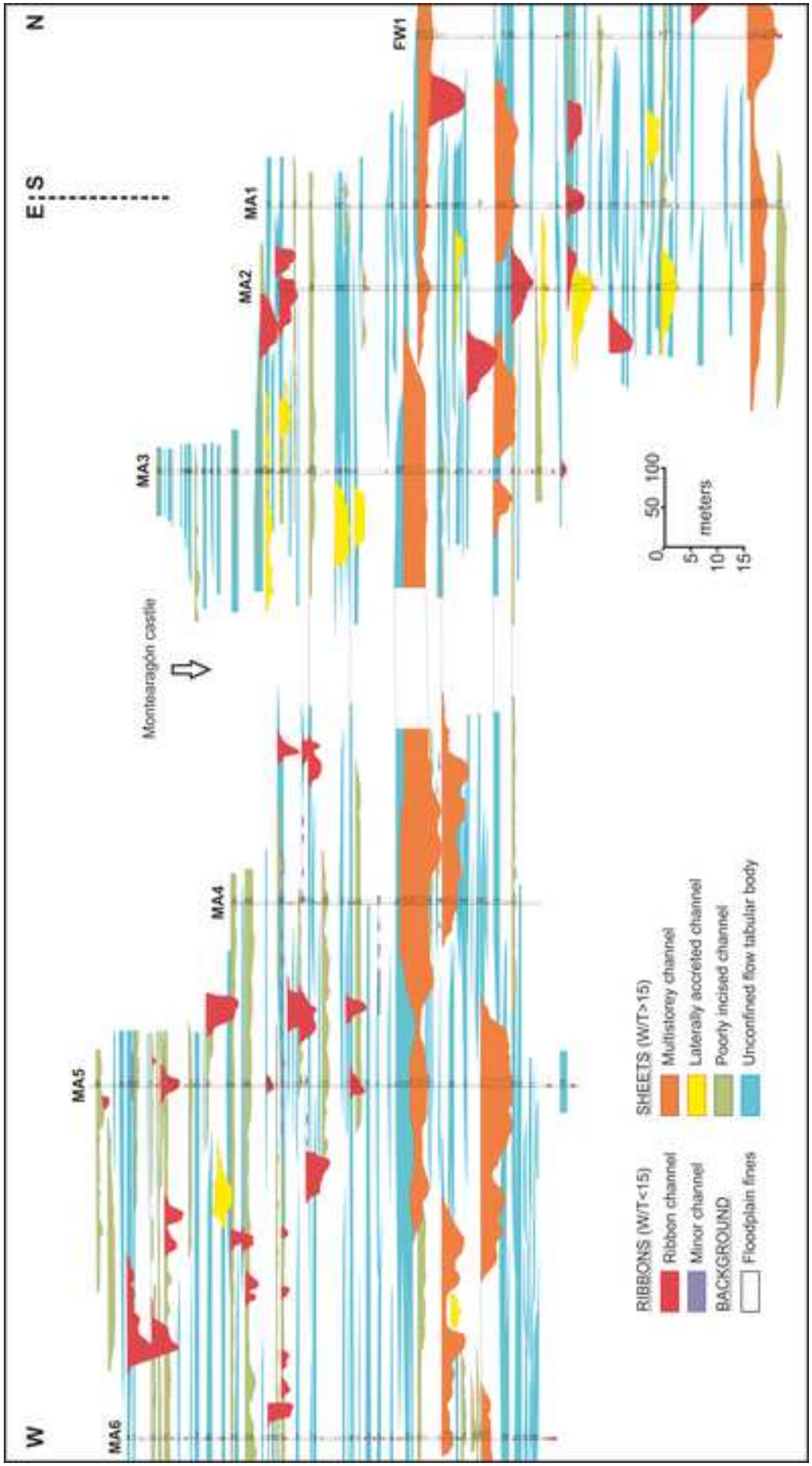

Table 1

TABLE 1. HIERARCHY AND CHARACTERISTICS OF THE BOUNDING SURFACES FOR FLUVIAL DEPOSITS

| Surface order | Time scale of process (years) | Characteristics and nature of bounding surfaces | Fluvial depositional units | Significance and example of processes |
|---|---|---|---|---|
| **1st** | $10^{-6}$-$10^{-3}$ | Lamination/set bounding surface | Lamina, ripple | Migration of dune bedforms under steady flow conditions. |
| **2nd** | $10^{-2}$-$10^{-1}$ | Coset bounding surface | Mesoform (dune) | Change in hydrodynamic conditions through time, related to short-term unsteady flow or local non-uniformity |
| **3rd** | $10^{0}$-$10^{1}$ | Inclined erosion surfaces within coset or group of cosets, dipping 5-20º in direction of accretion | Macroform growth increment | Medium-term change in hydrodynamic conditions related to stage fluctuation or major shifting of flow across/around a bar form (e.g. seasonal events, 10-year floods) |
| **4th** | $10^{2}$-$10^{3}$ | Separates units with discrete accretionary integrity (e.g. convex-up macroform top, minor channel scour, flat surface bounding floodplain elements) | Macroform (point bar, levee, splay, inmature paleosol) | Shift of bar/subchannel pattern related to inherent channel-floor instability or to reorganization during a major flood (e.g. 100-year floods, channel and bar migration) |
| **5th** | $10^{3}$-$10^{4}$ | Laterally extensive and with a marked shift in grain size, bedform scale, etc. (e.g. flat to concave-up channel base) | Channel, delta lobe, mature paleosol | Long-term geomorphic processes (e.g. shifting and erosion of a channel floor, isolated channels with relief reflecting channel avulsion or extensive surfaces within larger sandbodies recording channel migration) |
| **6th** | $10^{4}$-$10^{5}$ | Regionally extensive and separating major channel sandbodies from contrasting facies (fine-grained sediment or contrasting channel facies) | Channel belt, alluvial fan, minor sequence | Major change of fluvial regime, recording shifts of base level, climatic changes (5th-order, Milankovitch cycles) or fault pulses |
| **7th** | $10^{5}$-$10^{6}$ | Sequence boundary; flat, regionally extensive, or base of incised valley | Major depositional system, fan tract, sequence | 4th-order (Milankovitch) cycles or response to fault pulses |
| **8th** | $10^{6}$-$10^{7}$ | Regional disconformity | Basin-fill complex | 3th-order cycles by response to tectonic and eustatic processes |

*Note:* Designed by combining information from Miall (1996) and Reading (1996).

Table 2

TABLE 2. DIFFERENCES BETWEEN THE THICKNESSES MEASURED IN THE FIELD AND IN THE DOM FOR EACH STRATIGRAPHIC LOG, ALONG WITH OTHER FACTORS THAT MAY INFLUENCE ON THE MEASUREMENTS

| Log name | Measured thickness* (m) | Real thickness† (m) | Absolute error (m) | Relative error (%) | Orientation § (°) | Mean slope† (%) | Channel proportion# (%) | Sst. proportion# (%) |
|---|---|---|---|---|---|---|---|---|
| **FW1** | 67.10 | 68.18 | -1.08 | -1.58 | 48.43 | 0.48 | 13.59 | 28.05 |
| **MA1** | 93.10 | 95.87 | -2.77 | -2.89 | 56.23 | 0.36 | 13.80 | 33.68 |
| **MA2** | 96.00 | 97.62 | -1.62 | -1.66 | 57.08 | 0.34 | 22.79 | 41.22 |
| **MA3** | 73.60 | 75.29 | -1.69 | -2.24 | 37.08 | 0.34 | 9.75 | 35.54 |
| **MA4** | 54.00 | 56.88 | -2.88 | -5.06 | 64.03 | 0.33 | 16.32 | 41.41 |
| **MA5** | 87.40 | 90.36 | -2.96 | -3.28 | 6.18 | 0.48 | 22.44 | 44.69 |
| **MA6** | 75.70 | 78.80 | -3.10 | -3.93 | 30.54 | 0.49 | 8.48 | 31.61 |
| ***Mean*** | *78.13* | *80.43* | *-2.30* | *-2.95* | *42.80* | *0.40* | *15.31* | *36.60* |

*Measured assuming horizontal stratification.

†Calculated from the DOM.

§Regarding the stratigraphic maximum dip direction provided by the Virtual Datum (236.51°).

#Calculated from the logs.